Physica D 460 (2024) 134033

Contents lists available at ScienceDirect

Physica D

journal homepage: www.elsevier.com/locate/physd

On the collision dynamics in a molecular model

Esther Barrabés [a], Mercè Ollé [b,c,d], Óscar Rodríguez [b,c,*]

[a] Dept. Informàtica, Matemàtica Aplicada i Estadística, Universitat de Girona, 17003 Girona, Spain
[b] Dept. Matemàtiques, Universitat Politècnica de Catalunya, Av Diagonal 647, 08028 Barcelona, Spain
[c] IMTech, Universitat Politècnica de Catalunya, Pau Gargallo 14, 08028 Barcelona, Spain
[d] CRM, Campus de Bellaterra Edifici C, 08193 Bellaterra, Spain

ARTICLE INFO

Communicated by A. Celletti

Keywords:
Regularization
Ejection–collision orbits
Continuation of families
Bifurcations

ABSTRACT

We study the problem of the hydrogen atom submitted to a circularly polarized microwave field. This problem, analyzed from a classical mechanics approach, can be modeled by an autonomous Hamiltonian depending on one parameter $K > 0$. The paper is focused on the so called n-ejection–collision orbits (n-EC orbits), that is orbits that the electron describes when it ejects from the nucleus and collides with it at the n relative minimum in the distance with respect to the nucleus. In this work, we analyze the evolution of the families of n-EC orbits. We conduct a comprehensive numerical analysis of the bifurcations, which involves multiple precision computations, to characterize the successive bifurcation families that emerge. Additionally, we examine the periodic and quasi-periodic motion of the n-EC orbits belonging to these bifurcation families.

1. Introduction

In atomic physics one challenging problem is the interaction of atomic hydrogen with intense electromagnetic fields. We consider the case of a two-dimensional model of a hydrogen atom under a circularly polarized microwave field (CP problem). The problem, as well as the case of a linear field, or the case in which the field is elliptically polarized, has been studied using classical dynamical systems tools, with special emphasis on the mechanisms that explain ionization. More concretely, in the case of the circularly polarized microwave perturbation, it can be shown that the electron can make any desired number of excursions to long distances to the nucleus, and return to its vicinity, before actually leaving the system (ionizing). See, for example, [1–5] and the references therein for further details.

In [3] the authors discuss over the role of collisions on the process of ionization. In the linearly polarized microwave system, core collisions are a relevant mechanism to explain ionization, while in the case of the CP problem it seems that close encounters are not enough to cause ionization. Nevertheless, in [5] the authors show slow ionization through erratic orbits in which the electron makes multiple large distance excursions away from the nucleus with each one being followed by a close approach to the nucleus. The responsible for that slow ionization are the invariant manifolds associated to some hyperbolic invariant objects.

The CP problem can be regarded as a Hamiltonian problem that describes the motion of a particle under a specific potential, in a similar way as classical Celestial Mechanics problems of N bodies under Newtonian gravitational attraction. In all of these problems, a particular critical point is to understand the dynamics near collisions (partial or total). This is typically done by introducing a change of variables that regularizes the collision. One of the most classical regularization comes from McGehee's variables [6,7], that allows to transform the collision into an invariant manifold, which typically contains hyperbolic equilibrium points or periodic orbits. In this way, the orbits that emanate from collision are solutions on the unstable invariant manifolds associated to them, whereas the ones tending to collision belong to the stable manifolds. That is the approach of [8], where the author analyzes the ejection/collision orbits in the CP problem. In such a case the ejection/collision manifold is a torus and any ejection–collision (EC) orbit is a heteroclinic connection between two equilibrium points, which means, in particular, an infinite time to eject from/collide with the origin. This is clearly a disadvantage from a numerical point of view. Moreover, the initial conditions on these heteroclinic orbits are taken in an approximate way using an approximated parametrization of the invariant manifolds, starting not at the ejection/collision but close to it.

Finally, let us remark that ejection/collision orbits also play an important role in other physical problems such as astronomy or celestial mechanics. There are numerous analytical works on the existence of EC orbits, for the specific case of 1-EC (see Definition 1 of n-EC) in different

* Corresponding author at: Dept. Matemàtiques, Universitat Politècnica de Catalunya, Av Diagonal 647, 08028 Barcelona, Spain.
E-mail address: oscar.rodriguez@upc.edu (Ó. Rodríguez).

https://doi.org/10.1016/j.physd.2023.134033
Received 12 October 2023; Received in revised form 16 December 2023; Accepted 19 December 2023
Available online 19 January 2024

problems, see for example [9–15]. More recently, numerical and analytical results have been obtained for the general case of n-EC orbits in the RTBP [16–19] and for other phenomena such as the connections of EC orbits with invariant objects [20] and generalized periodic solutions [21,22].

Our objective in this paper is to gain insight in the dynamics close to collision in the CP problem, and analyze the behavior and evolution of the families of n-EC orbits, with a particular emphasis on the properties and characteristics of the bifurcation families that arise as the energy levels of the problem vary. We apply the Levi-Civita regularization which presents two clear advantages compared with the McGehee's one: (i) the EC orbits require a finite interval of time, (ii) and the initial conditions are exact on the collision point. Using Levi-Civita variables and following the ideas introduced in [19], we can analytically prove the existence of two families of n-EC orbits for any $n \in N$, provided that the Jacobi constant is sufficiently large.

We follow numerically these two families found analytically, and describe the structure of them, as well as the description of the bifurcations that appear along the way as the value of C decreases, where C is the Jacobi constant, related to the energy H by $C = -2H$. In particular, we compute the limit value of C, $\hat{C}$, for which there exist two and only two n-EC orbits (for higher values of C) and we provide an analytical expression for that $\hat{C}$. Finally, special attention is devoted to quasi-periodic and periodic behavior of the n-EC orbits.

The paper is organized as follows: in Section 2 we deduce the system of ordinary differential equations (ODEs) for the motion of the electron in a rotating system of coordinates. Several properties that will be useful for analyzing n-EC orbits are recalled and we provide the regularized ODEs using the Levi-Civita variables. In Section 3, we present the n-EC orbits, the tools we will use to study them and the analytical result that we can derive by following the ideas from [19]. Section 4 is devoted to the numerical simulations: continuation of the two (main) families of n-EC orbits – guaranteed by the analytical results –, the computation of $\hat{C}$ and to analyze the first bifurcation of one of the families. In Section 5 we analyze other bifurcations that appear along the continuation of the two main families. Such numerical simulations have been done using double, quadruple and even multiple precision computations (when necessary); the systems of ODE are integrated with own implemented Runge–Kutta 78 (see [23]) and Runge–Kutta 89 (see [24]) methods with an adaptive step size described in [25], and a Taylor method implemented on a robust, fast and accurate package by Jorba and Zou [26].

2. The CP problem. Main properties

We consider the relative motion of a hydrogen atom submitted to a circularly polarized (CP) microwave, where the pulse of the microwave field is taken with a *flat-top* shape, that is, the field amplitude is ramped up in time until it achieves a final, constant amplitude. In this study we ignore the ramping and just consider the dynamics after the flat-top has been reached (see [3] for a discussion of the consequences of the initial ramp). See [3–5] for a detailed derivation of the model and its properties.

We consider a reference system where the nucleus of the hydrogen atom is at the origin. The dynamics of its electron in the limit of an infinitely massive nucleus and in atomic units $m_e = \bar{h} = e = 1$ subjected to a CP microwave field is described as a Hamiltonian system through

$$\tilde{H}(X, Y, Z, X', Y', Z') = \frac{1}{2}(X'^2 + Y'^2 + Z'^2) - \frac{1}{R} + F(X\cos(\omega\tau) + Y\sin(\omega\tau)), \tag{1}$$

where (X, Y, Z) are the position coordinates of the electron, $R^2 = X^2 + Y^2 + Z^2$, τ is the time, $' = \frac{d}{d\tau}$, ω is the angular frequency of the microwave field and $F > 0$ is the field strength. We consider the motion in the planar case $Z = 0$. Furthermore, we take a rotating frame with the CP field, that is, we introduce (x, y) coordinates such that

$$\begin{pmatrix} X \\ Y \end{pmatrix} = \begin{pmatrix} \cos(\omega\tau) & -\sin(\omega\tau) \\ \sin(\omega\tau) & \cos(\omega\tau) \end{pmatrix} \begin{pmatrix} x \\ y \end{pmatrix}.$$

Then, the Hamiltonian (1) transforms into an autonomous Hamiltonian given by

$$\tilde{H}(x, y, p_x, p_y) = \frac{1}{2}(p_x^2 + p_y^2) - \omega(xp_y - yp_x) - \frac{1}{R} + Fx, \tag{2}$$

where $R = \sqrt{x^2 + y^2}$, $p_x = x' - \omega y$ and $p_y = y' + \omega x$.

In order to simplify this Hamiltonian we introduce a rescaling in time $t = \omega\tau$ and a symplectic change of coordinates with multiplier $\omega^{-1/3}$ given by

$$(x, y) = \omega^{2/3}(\hat{x}, \hat{y}), \quad (p_x, p_y) = \omega^{1/3}(p_{\hat{x}}, p_{\hat{y}}), \tag{3}$$

so that the Hamiltonian (2) in the new variables (we drop the hat notation for simplicity) is

$$H(x, y, p_x, p_y) = \frac{1}{2}(p_x^2 + p_y^2) - xp_y + yp_x - \frac{1}{r} + Kx, \tag{4}$$

with $K = F/\omega^{4/3}$, $r = \sqrt{x^2 + y^2}$, $p_x = \dot{x} - y$, $p_y = \dot{y} + x$ and $\dot{} = \frac{d}{dt}$. From now on we call (x, y) the synodical coordinates.

We remark that the Hamiltonian obtained (4) has two degrees of freedom, depends on a single parameter $K > 0$ and is expressed as a perturbation (the term Kx) of the well known Kepler problem in rotating coordinates.

The system of ordinary differential equations (ODE) associated with the Hamiltonian H (4) is

$$\begin{cases} \ddot{x} - 2\dot{y} = \Omega_x(x, y), \\ \ddot{y} + 2\dot{x} = \Omega_y(x, y), \end{cases} \tag{5}$$

where

$$\Omega(x, y) = \frac{1}{2}r^2 + \frac{1}{r} - Kx, \tag{6}$$

and $r = \sqrt{x^2 + y^2}$.

System (5) has some interesting properties for our purposes:

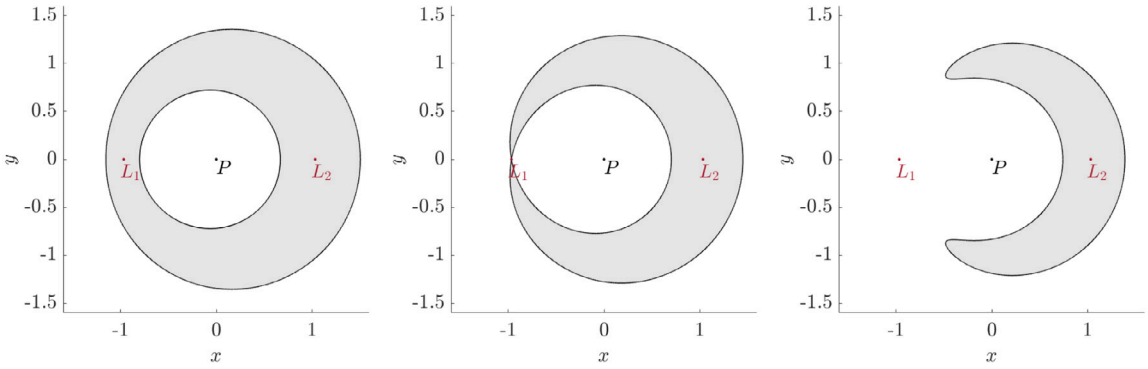

Fig. 1. Hill regions for $K = 0.1$ and $C > C_{L_1}$, $C = C_{L_1}$ and $C < C_{L_1}$ (from left to right). P denotes the nucleus located at the origin.

1. It has the symmetry:

$$(t, x, y, \dot{x}, \dot{y}) \to (-t, x, -y, -\dot{x}, \dot{y}). \tag{7}$$

   A geometrical consequence is that, given an orbit in the configuration plane (x, y) described in forward time, there exists another orbit in the (x, y) plane which is symmetrical with respect the x axis and described in backward time.
2. It has two equilibrium points denoted by L_i located in the configuration space at $(x_{L_i}, 0)$, $i = 1, 2$ with $x_{L_1} < 0$ and $x_{L_2} > 0$. Concerning their stability, L_1 is a center–saddle for any value $K > 0$; L_2 is a center–center for $K \leq K_{crit}$ and a complex saddle for $K > K_{crit}$, being $K_{crit} = \frac{3^{-4/3}}{2} \approx 0.11556021$. See details in [5].
3. It has a first integral, called Jacobi first integral, given by

$$C = 2\Omega(x, y) - (\dot{x}^2 + \dot{y}^2). \tag{8}$$

4. For a fixed value of K and the first integral C, the admissible regions of motion, known as Hill regions, are given by

$$\mathcal{R}(C) = \{(x, y) \in \mathbb{R}^2 \,|\, 2\Omega(x, y) \geq C\}. \tag{9}$$

   We denote by C_{L_i} the value of C at the equilibrium point L_i, $i = 1, 2$. As L_i are critical points of the potential (6), the topology of the Hill's regions change at C_{L_i}. In Fig. 1 we plot the topology of the Hill regions for different values of C.
5. Due to the Lyapunov theorem (see [27]), for any value of $K > 0$ there exists a family of Lyapunov periodic orbits around L_1 when varying C. For any value of $K \in (0, K_{crit})$ there exist two families of periodic orbits around L_2 (when the eigenvalues are not proportional) and for $K > K_{crit}$, although L_2 is a complex saddle, there exists a family of periodic orbits due to a Hopf bifurcation that takes place (see [28]).

It is clear that system (5) has a singularity at the origin $x = y = 0$, that is, when $r = 0$; we will say from now on *a collision with the origin*. Precisely this paper is focused on orbits that eject from (or collide with) the origin, called ejection (collision orbits). See a formal definition in next Section. Therefore, we need to regularize this singularity in order to deal with it. To do so, there are different possibilities to consider (see for example [29]). Here we use the Levi-Civita regularization, which turns out to be a good choice both for analytical and numerical purposes. This regularization consists in a transformation of coordinates and time given by

$$\begin{cases} x = u^2 - v^2, \\ y = 2uv, \\ \dfrac{dt}{ds} = 4(u^2 + v^2). \end{cases} \tag{10}$$

In these coordinates, the regularized system (5) becomes

$$\begin{cases} u'' - 8(u^2 + v^2)v' = \left(4(u^2 + v^2)U\right)_u = -4Cu - 16Ku^3 + 12(u^2 + v^2)^2 u, \\ v'' + 8(u^2 + v^2)u' = \left(4(u^2 + v^2)U\right)_v = -4Cv + 16Kv^3 + 12(u^2 + v^2)^2 v, \end{cases} \tag{11}$$

where $' = d/ds$ and

$$U(u, v) = \frac{1}{2}(u^2 + v^2)^2 + \frac{1}{u^2 + v^2} - K(u^2 - v^2) - \frac{C}{2}. \tag{12}$$

We notice that the system (11) has no singularities, is polynomial and it is defined for each value of the Jacobi first integral C fixed.
In a similar way as system (5), system (11) has the following properties:

1. As the Levi-Civita transformation duplicates the configuration space, the equilibrium points are also duplicated and they are located on the plane (u, v). See Fig. 2.
2. Moreover, the equations of motion satisfy an extra symmetry, that is,

$$(s, u, v, u', v') \to (-s, u, -v, -u', v'), \tag{13a}$$

$$(s, u, v, u', v') \to (-s, -u, v, u', -v'). \tag{13b}$$

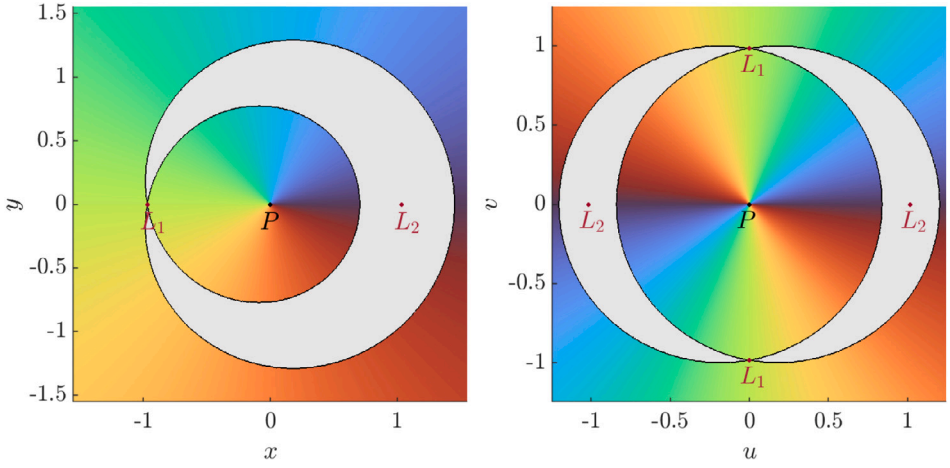

Fig. 2. Hill region for $K = 0.1$ and $C = C_{L_1}$ in synodical (left) and Levi-Civita (right) coordinates. The gradient of colors represents the angle with respect to the position of the first primary in the original (x, y) synodical coordinates. In gray the forbidden region.

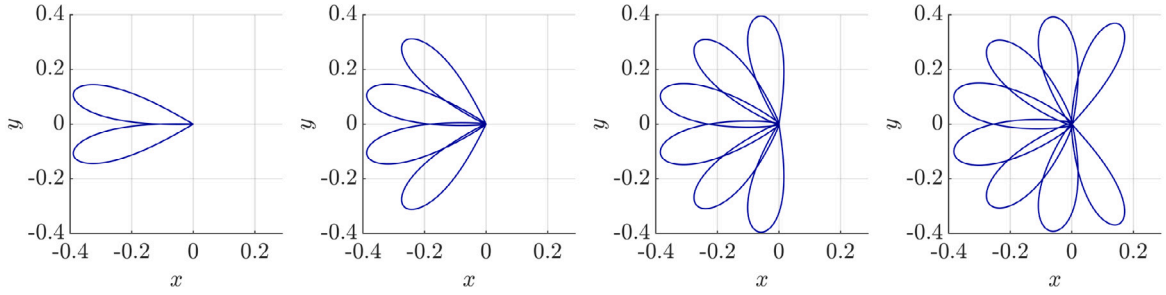

Fig. 3. Trajectories of n-EC orbits for $n = 2, 4, 6, 8$ (from left to right), $K = 0.1$ and $C = 5$.

3. The integral of motion (8) is given by the relation

$$u'^2 + v'^2 = 8\left(u^2 + v^2\right)U, \tag{14}$$

which is regular at the collision with the origin $(u = 0, v = 0)$. In particular the velocity at this point satisfies:

$$u'^2 + v'^2 = 8. \tag{15}$$

4. Given a value of C, the possible region of motion in (u, v) variables now becomes

$$\mathcal{R}(C) = \left\{(u, v) \in \mathbb{R}^2 \mid (u^2 + v^2)U \geq 0\right\}. \tag{16}$$

See Fig. 2.

5. The existence of the Lyapunov orbits, of course, remains the same.

3. *n*-Ejection–collision orbits. Characterization and analytical results

We start defining an ejection (collision) orbit as that trajectory that ejects from (collides with) the origin. From (14) we know the velocity relation at any point, and in particular at the origin. So we can define, for any given value of $K > 0$, the ejection (collision) orbits manifold W^e (W^c) of energy level C as the sets of orbits that have initial (final) conditions

$$(u(0), v(0), u'(0), v'(0)) = (0, 0, 2\sqrt{2}\cos\theta_0, 2\sqrt{2}\sin\theta_0), \qquad \text{for any} \quad \theta_0 \in [0, \pi) \tag{17}$$

integrated forward (backward) in time. Notice that, due to the doubling configuration plane in Levi-Civita variables, there is no need to consider $\theta_0 \in [0, 2\pi)$. Therefore, given K and C, an ejection (collision) orbit is characterized by θ_0. An ejection–collision (EC) orbit is an orbit that belongs to $W^e \cap W^c$.

In this work, we will focus on a specific type of ejection–collision orbits, the so called n-ejection–collision orbits, defined as follows.

Definition 1. An n-ejection–collision (n-EC) orbit is the orbit that describes the electron when it ejects from the nucleus and collides with it at the n relative minimum in the distance with respect to the origin.

Remark. The definition of the n-EC orbits implies that the orbits describe n relative maxima in the distance with respect to the origin before colliding in the n relative minimum with it. This characterization allows us to have a more visual characterization of the n-EC orbits (see for example Fig. 3).

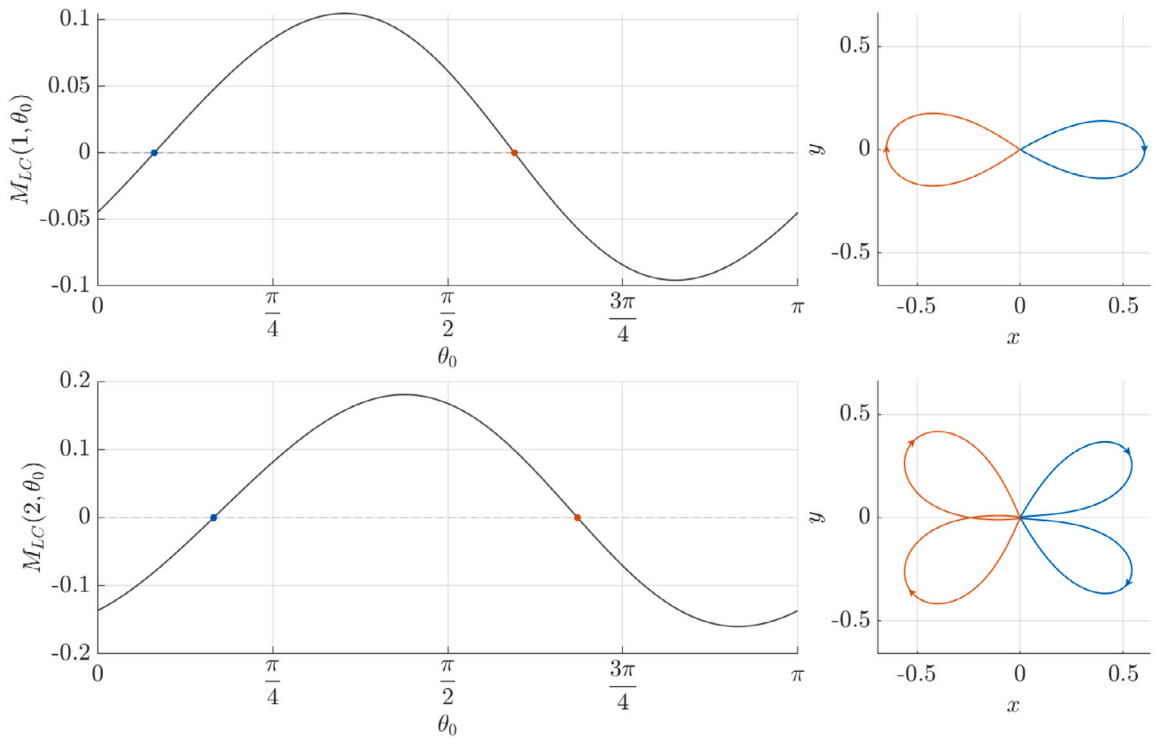

Fig. 4. $K = 0.1$, $C = C_{L_1}$. Left. Curve $(\theta_0, M_{LC}(n,\theta_0))$, for $n = 1, 2$. Right. The two corresponding n-EC orbits on the (x, y) projection.

It is well known that collisions in N body problems (an ejection can be viewed as a collision backwards in time) are related to zero angular momentum, see for example the nice revision about collisions in N-body problems by Saari [30]. In fact, collision orbits have zero angular momentum at the collision. In synodic coordinates the angular momentum writes $M = x\,y' - y\,x'$. In a similar way we can define directly the angular momentum in Levi-Civita coordinates as

$$M_{LC} = uv' - vu'. \tag{18}$$

Next, let us provide the following result that characterizes the collision based on the value of the angular momentum.

Proposition 1. *A solution of system (11) is a collision orbit if and only if it satisfies that at a minimum in the distance to the origin the angular momentum M_{LC} is equal to zero and $u'^2 + v'^2 \neq 0$.*

Proof. First, it is clear that if a collision takes place, $u = v = 0$, the distance is at a minimum and $M_{LC} = 0$ is trivially satisfied. Notice also that at collision, using the Jacobi integral (15) we have that $u'^2 + v'^2 = 8 \neq 0$.

Next, suppose that $M_{LC} = 0$, $u'^2 + v'^2 \neq 0$ and the distance to the origin is at a minimum. In particular, (u, v, u', v') is a critical point of the distance function, that is,

$$uu' + vv' = 0. \tag{19}$$

Suppose that $v' \neq 0$ (the same argument applies if $u' \neq 0$). Then, from $M_{LC} = 0$ we have that $u = vu'/v'$ and by (19)

$$\frac{vu'}{v'}u' + vv' = 0 \Longrightarrow vu'^2 + vv'^2 = v(u'^2 + v'^2) = 0 \Longrightarrow v = 0,$$

and then also $u = 0$, so we are at a collision. This concludes the proof. □

This characterization for detecting collisions, based on angular momentum computation, is crucial for our study of n-EC orbits. In this manner, let us introduce the subsequent definition:

Definition 2. For a fixed value of K and C we define $M_{LC}(n,\theta_0)$ as the value of the angular momentum (18) of the ejection orbit with ejection angle θ_0 at the nth minimum in the distance to the nucleus.

It is important to note that from Proposition 1, we can see that the zeros of $M_{LC}(n,\theta_0)$ correspond to the n-EC orbits, which will have an ejection angle θ_0 (see Lemma 1 in Appendix A for technical details). Therefore, the problem of computing n-EC orbits is analogous to finding the zeros of $M_{LC}(n,\theta_0)$ (see Fig. 4).

Furthermore, by following a procedure similar to the one introduced in [19] for computing the zeros of $M_{LC}(n,\theta_0)$, we can obtain the following analytical result:

Theorem 1. *Assume a given value of $K > 0$. Then, there exists a value $\hat{L}$ such that for $L \geq \hat{L}$ and any $n \in \mathbf{N}$, for $C = Ln^{2/3}$ there exist exactly two n-EC orbits of the CP problem given by (11). In the (x, y) projection, each n-EC orbit is symmetric with respect to the x axis.*

Remark 1. It is worth noting that the constant $\hat{L}$ in the Theorem is independent of the value of n. Therefore, the dependence of $\hat{C} = \hat{L}n^{2/3}$ in n is expressed explicitly and, as we will see in Section 4, the analytical expression obtained coincides with the numerical results.

Remark 2. The values of C considered in the analytical results will typically satisfy $C > C_{L_1}$. This condition guarantees that the dynamics is only possible in a confined region around the origin, and is quite simple. See Fig. 1 left.

Definition 3. Given $K > 0$ and n, when varying the Jacobi constant C, two different families of n-EC orbits are obtained. We define them families α_n and β_n.

The general idea of the proof is that through the regularization of Levi-Civita, a change of coordinates involving the new definition of C as $C = Ln^{2/3}$ and a rescaling of time, we can separate the dynamics of the two-body problem ($K = 0$) from the perturbation. Treating it as a fixed-point problem, applying Proposition 1 that allows us to detect collisions based on angular momentum and applying the Implicit Function Theorem, we conclude that there exist two n-EC orbits under the assumptions described in Theorem 1. The symmetry of these orbits is a consequence of the problem's inherent symmetry (13). The details can be found in Appendix A and follows the concepts introduced in [19].

4. Numerical extension

The analytical result of Theorem 1 only provides us with results for values of C that are sufficiently large, so the natural step is to complement such result from a numerical point of view. More concretely:

(i) For any given value of $K > 0$ and $n > 0$, we compute and continue numerically both families of n-EC orbits α_n and β_n (see Definition 3). We take the value of C as the parameter of continuation of both families.

(ii) Theorem 1 claims the existence of the two families, for any n given provided that C is big enough. On one hand, we consider values of C not necessarily big. On the other hand, the Theorem claims that both families exist if $C \geq \hat{C}$, where $\hat{C} = \hat{L}n^{2/3}$, for some suitable value of $\hat{L}$. However, no specific value of $\hat{C}$ (or equivalently $\hat{L}$) is obtained from the analytical proof. Precisely, this value of $\hat{C}$ is the bifurcation value of C for which the first bifurcation takes place, for each fixed value of n. We compute such limit constant value $\hat{C}$, and we also provide an analytical expression that fits the value of $\hat{C}$.

(iii) We analyze the bifurcations that appear when doing the continuation of the families for $K > 0$ and n fixed and decreasing the value of C. That is, for smaller values of C, there exist more than two n-EC orbits. We discuss some particularities of the *first* bifurcating family, which has two branches, and we describe the properties concerning periodicity and symmetry of their n-EC orbits. Moreover, we explain the relation between some n-EC orbits of the bifurcated branches and families of periodic (non EC) orbits.

Remark. Along this Section we will always assume $C \geq C_{L_1}$ (see Figs. 1 and 2).

4.1. Numerical computation of the families α_n and β_n of n-EC orbits

In order to compute an n-EC orbit, for a value of $K > 0$, n and C (big) given, we will use Proposition 1. Starting at an ejection with initial conditions (17), we have a unique trajectory, which is an ejection orbit. We numerically integrate the system (11) along time until the trajectory reaches the nth minimum distance to the origin with $u'^2 + v'^2 > 0$. At this particular instant of time we compute the angular momentum. Varying the initial condition $\theta_0 \in [0, \pi)$, we obtain the curve $M_{LC}(n, \theta_0)$ and we look for its zeros, see Fig. 4. To compute the numerical extension of the families α_n and β_n, we will use the following approach: having set a value of $K > 0$ and C large enough, for a fixed n, we will evaluate $M_{LC}(n, \theta_0)$ on a grid of values $\theta_0 \in [0, \pi]$. From this grid, using a Newton method, we can easily determine the starting conditions of the ejection–collision orbits (corresponding to the solutions θ_0^* of $M_{LC}(n, \theta_0) = 0$) as well as the required time s^* of those to reach collision. Next, by fixing a smaller value of C and using the previous values (θ_0^*, s^*) as a starting point, we can find the conditions for this new value of C with a Newton method. Finally, we extend both families in (C, θ_0, s) using the arc parameter as an additional equation. We show the result of this computation in Fig. 5, for $K = 0.1$, $C \in [C_{L_1}, 6]$ and $n = 1$. The two curves α_1 and β_1 (plot on the right) correspond to points where both conditions $M_{LC}(n, \theta_0) = 0$ and $u'^2 + v'^2 > 0$ are satisfied. The blue curve corresponds to family α_1 and the red one to family β_1. The graded color blue and red of the curves help to identify the two 1-EC orbits associated with each value of C (see the projection in the configuration coordinates (x, y), left plot). We show in black the 1-EC orbits for $C = 4.5$.

4.2. First bifurcations

It is clear that numerically we can continue families α_n and β_n (existing for C big enough) for decreasing values of C. In doing so, bifurcations naturally appear. The purpose of this Subsection is to focus our attention on the *first* bifurcation of each family. Before doing so, let us make a comment about periodic ejection–collision orbits, that will appear naturally when studying bifurcations.

Given an EC orbit, let us define θ_f as the polar angle of the velocity vector (in Levi-Civita coordinates) at the collision. Actually we may have two different cases:

(i) $\theta_0 = \theta_f$, then the EC orbit will be periodic of period T in (u, v) coordinates (being T the time spent from ejection to collision). See Fig. 6 top, where the periodic EC orbit (in purple or in red) are plotted both in Levi-Civita (u, v) coordinates and synodical ones (x, y). Note that both LC orbits correspond to the same synodical one. We clearly see that, in (u, v) coordinates, after describing three *petals* (that is, the number of maxima of the distance to the nucleus) the condition $\theta_0 = \theta_f$ is satisfied. Meanwhile, the orbit in (x, y) coordinates also describes three petals.

(ii) $|\theta_f - \theta_0| = \pi$, the orbit arrives at a collision with an angle such that $|\theta_f - \theta_0| = \pi$ in time T and due to the nature of Levi-Civita variables, in order to have a periodic orbit in (u, v) coordinates, a time equal to $2T$ is required. See Fig. 6 bottom where the ejection orbit describes not four but eight petals in order to be a periodic orbit. Meanwhile, the orbit in (x, y) variables is described twice (it bounces back after collision).

Let us remark that due to the symmetry of the problem, we know that the initial angle and the collision angle of the EC orbits of the α_n and β_n families satisfy the condition $\theta_0 = \pi - \theta_f \pmod{\pi}$. Therefore, when the initial angle of the orbits of these families is $k\pi/2$ with $k \in \mathbb{Z}$, we will have a periodic n-EC orbit.

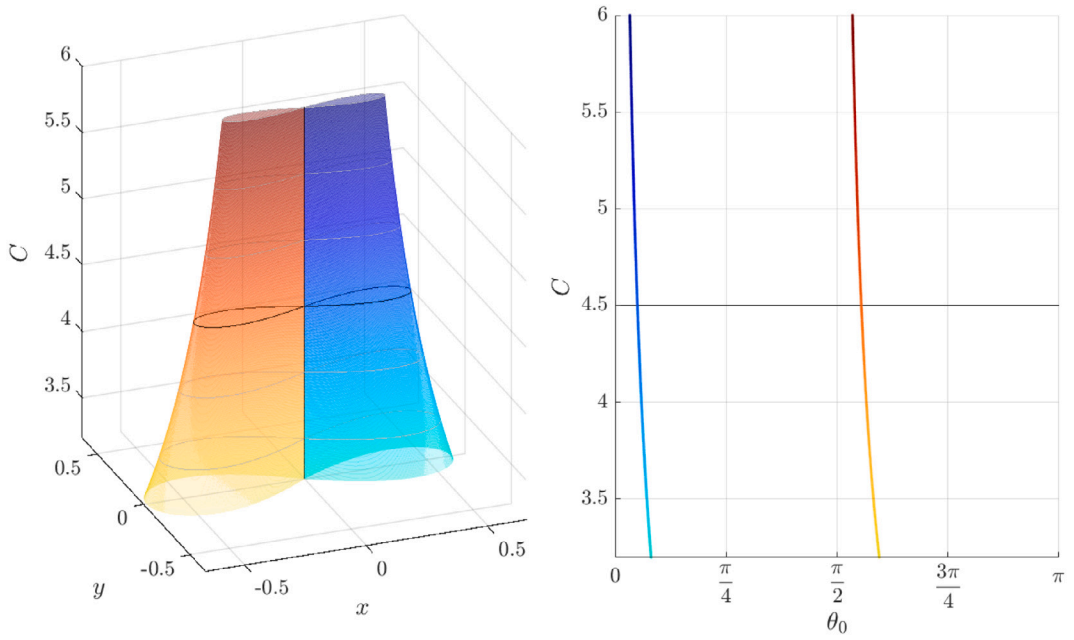

Fig. 5. Left: The (x, y) projection of the 1-EC orbits belonging to families α_1 (in blue) and β_1 (in red) for $C \in [C_{L_1}, 6]$ and $K = 0.1$. Right: The two families α_1 and β_1 are characterized by the variables (θ_0, C).

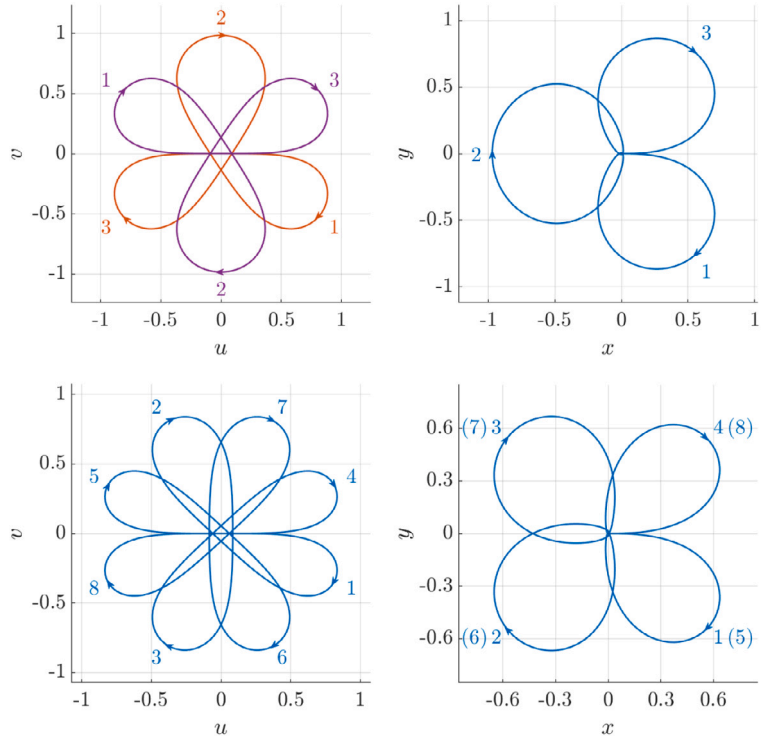

Fig. 6. Periodic EC orbits in Levi-Civita coordinates (left) or synodical ones (right). Top. Period T. Bottom. Period $2T$.

Next we describe the first bifurcation that takes place when doing the continuation of families α_n and β_n, varying C. We discuss the results obtained for $K = 0.1$, but, of course, the same kind of exploration can be done for any value of K. For the values explored $K \in (0, 1]$, we have obtained the same behavior.

In order to show the bifurcation, we plot in Fig. 7 the value of the function $M_{LC}(n, \theta_0)$, for $K = 0.1$, $C \in [C_{L_1}, 10]$ and $n = 5, 6, 7, 8, 9, 10$. The continuous black curves provide the values $M_{LC}(n, \theta_0) = 0$ corresponding to n-EC orbits (see Proposition 1).

Looking at Fig. 7, we remark that we clearly see the intersection between family α_n and $\theta_0 = \pi/2$ and the one of family β_n and $\theta_0 = 0 \pmod{\pi}$. We know that precisely for these values of θ_0, the corresponding n-EC orbit is periodic.

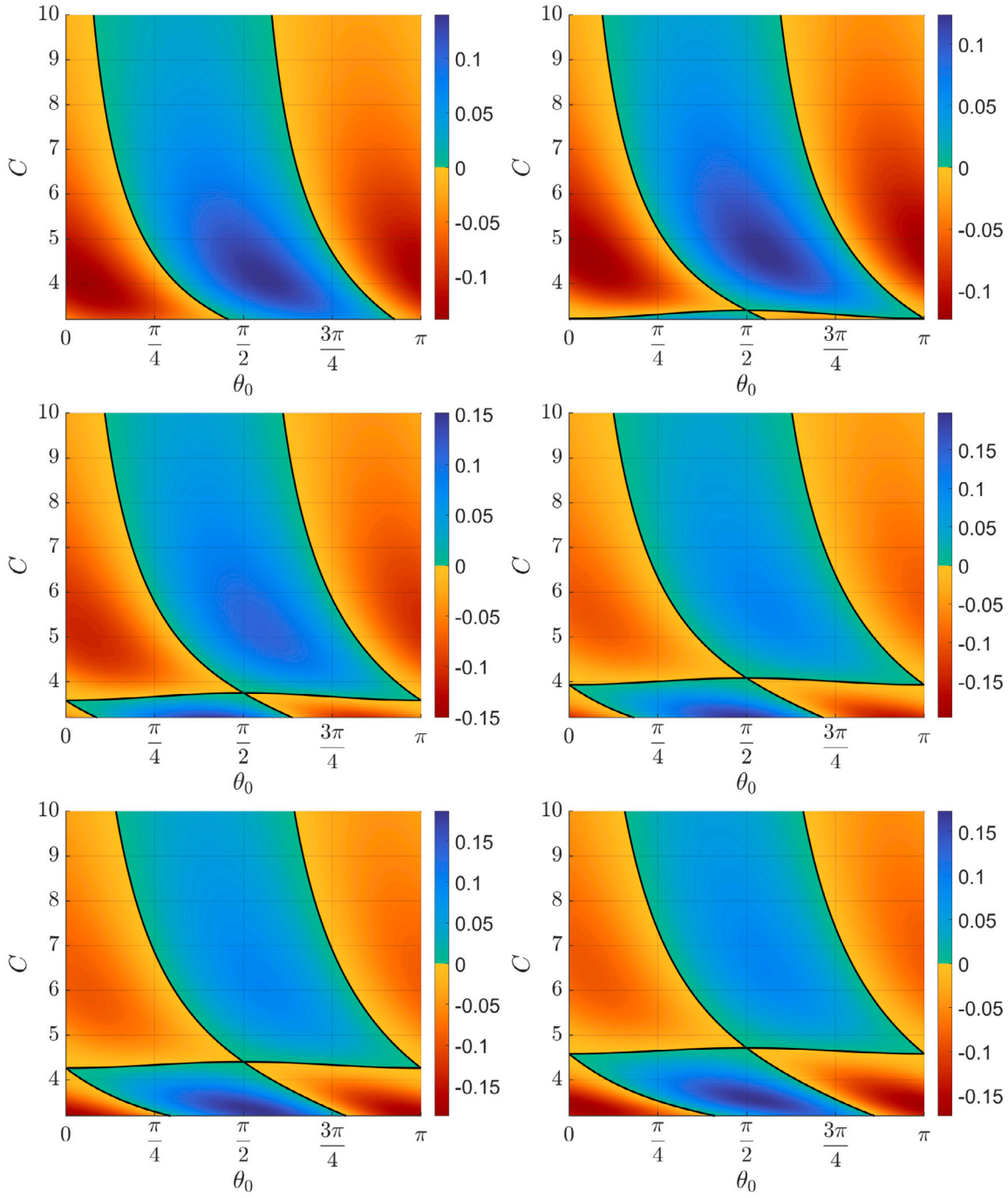

Fig. 7. Value of the angular momentum $M_{LC}(n,\theta_0)$ for $K=0.1$, $n=5,6,7,8,9,10$. In black, the values of (θ_0,C) at which $M_{LC}=0$.

Next, we describe the evolution of the bifurcating orbits of the first bifurcation family when doing the continuation of the two main families. On one hand, it is *apparent* that there is a bifurcating family, and the bifurcation *seems* to be at $\theta_0=\pi/2$, giving rise to two different branches that *seem to terminate* at family β_n for $\theta_0=\pi$ (mod π). See Fig. 7.

Let us focus on the first bifurcating family of n-EC orbits – appearing from the bifurcated orbit – for decreasing values of C, that is the almost horizontal curve for $\theta_0\in[0,\pi]$ bifurcating from the family α_n (see Fig. 7). The bifurcated family exists for a suitable range in C and for the whole range of $\theta_0\in[0,\pi]$. We denote by B_n the bifurcated family. Actually it consists of two branches, B_n^- and B_n^+. These two branches can be observed with more detail in Fig. 8 for $n=6$ and $K=0.1$ (the green and purple curves respectively). The two bifurcated branches emerge from family α_n *apparently* at $\theta_0=\pi/2$ and collapse into the family β_n *apparently* at $\theta_0=0$ (mod π).

From Fig. 8 it is *apparent* that when the orbit in the family α_6 is periodic (see trajectory ①, for $\theta_0=\pi/2$), the branches B_6^- (represented in green) and B_6^+ (represented in purple) emerge, both of which are symmetrical to one another (see trajectories ② and ③). These two branches *seem* to collapse into the orbit of the family β_6 with an initial angle of $\theta_0=0$ (or π) (see trajectory ④). We enumerate the petals to show the actual path along the EC orbits and also to see the evolution of the obits when decreasing C.

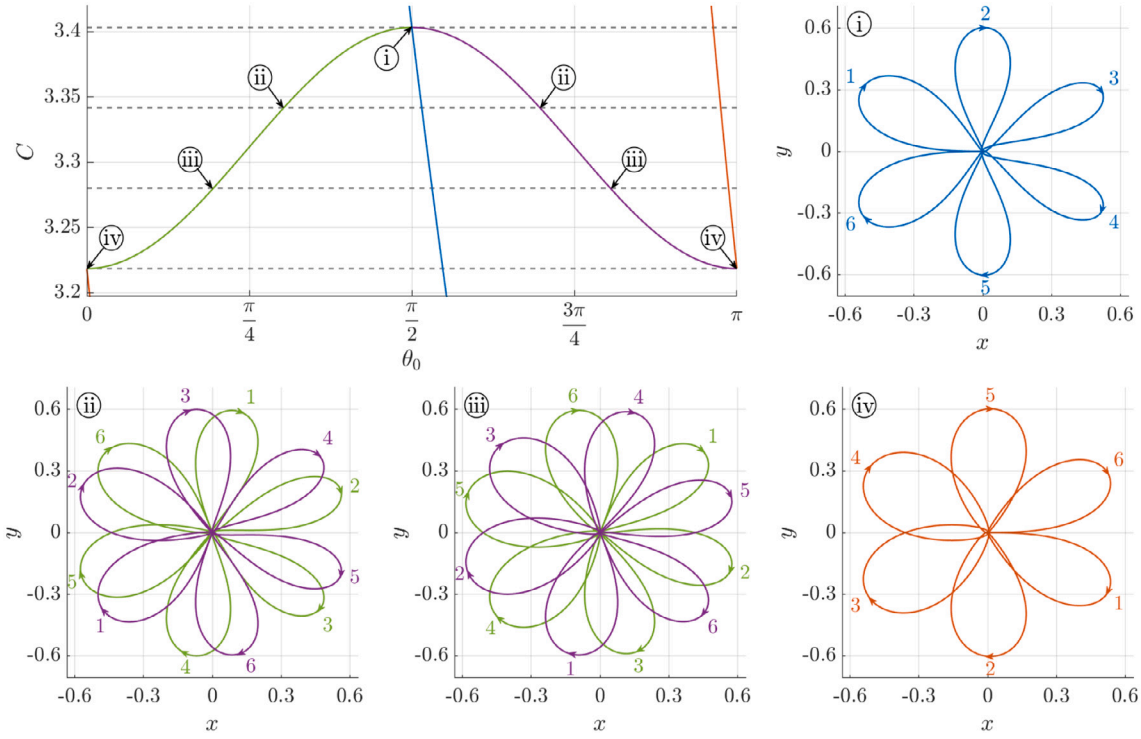

Fig. 8. Top left. Families α_6 (in blue), β_6 (in red) and the bifurcated branches (in green and purple). Top right. Periodic 6-EC orbit. Bottom. Orbits belonging to the two bifurcated branches. Orbit ⓘⓥ is a periodic 6-EC orbit. The orbits are plotted in synodical (x, y) coordinates.

Let us remark that due to the symmetry (13) of the problem, if there exists an orbit with ejection angle $\theta_0^1 \in [0, \pi)$ there will be another collision orbit with angle $\theta_f^2 = \pi - \theta_0^1$ –assuming from now on that we deal with angles modulus π due to the double covering of the Levi-Civita variables–. If we suppose that the orbits with initial angles $\theta_0^{1,2}$ are EC orbits, we have also that $\theta_f^1 = \pi - \theta_0^2$. That is:

$$\left.\begin{aligned} \theta_0^1 &= \pi - \theta_f^2 \pmod{\pi}, \\ \theta_0^2 &= \pi - \theta_f^1 \pmod{\pi}. \end{aligned}\right\} \tag{20}$$

From Figs. 7 and 8, it is *apparent* that the two branches, B_n^+ and B_n^-, exhibit symmetry with respect to the initial angle. In particular, it seems that the ejection angle θ_0^+ of the orbits from the branch B_n^+ and the ejection angle θ_0^- of the orbits of the branch B_n^- are symmetric with respect to $\pi/2$. This symmetry would imply, as discussed previously, that the orbits of branches B_n^+ and B_n^- correspond to families of periodic n-EC orbits. However, although this symmetry seems to exist, it really does not, that is, the n-EC orbits of the bifurcated branches B_n^- and B_n^+ are *not* periodic in general, but only $n-1$ specific orbits will be periodic. To provide numerical evidence of this assertion, we compute the difference between the initial and final angles of these orbits, that is the quantity

$$d(\theta_0, \theta_f) = \left[\theta_0 - \theta_f + \pi/2\right] \pmod{\pi} - \pi/2. \tag{21}$$

From the above discussion, the zeros of $d(\theta_0, \theta_f)$ correspond to periodic n-EC orbits. It turns out that we obtain exactly $n-1$ values of θ_0 such that $d(\theta_0, \theta_f) = 0$, that is, we have $n-1$ periodic n-EC orbits belonging to the families B_n^+ and B_n^-. This can be observed in Fig. 9 for the orbits of the B_n^- family where $d(\theta_0, \theta_f)$ is plotted as a function of the ejection angle for $n = 6, 7, 8, 9, 10, 11$ and $K = 0.1$. Therefore, given n, not all the n-EC orbits of the bifurcating branches are periodic, but only $n-1$ of them are periodic (those associated with the zeros of $d(\theta_0, \theta_f) = 0$). Note that as n increases, the range of values taken by d becomes extremely small, and it is necessary to work with multiple precision. Furthermore, as we will see later on, these $n-1$ periodic n-EC orbits are symmetric themselves and therefore, these $n-1$ periodic n-EC orbits of B_n^- and B_n^+ are the same. Moreover, we will show later on that they have one intermediate collision. This symmetry (so periodic) property does not happen for the remaining orbits of the two branches.

Therefore, the bifurcation family B_n is born from the family α_n at θ_0 close to $\pi/2$ and collapse at the family β_n at θ_0 close to 0 (mod π). This can be observed in Fig. 9.

The behavior observed in Fig. 9 can be explained through the existence of two families of self-symmetric periodic orbits (non EC orbits in general), one family composed of stable orbits and the other family of unstable ones. Along the evolution of each family (varying C) particular periodic orbits have collisions with the nucleus. Such EC orbits, that are self-symmetric and periodic, are precisely the only ones belonging to branches B_n^- and B_n^+ that are periodic.

In Fig. 10 top we schematically show the two families of periodic orbits (PO) varying the value of C (on the x axis). We also label from 1 to 7 precisely the orbits belonging to one family or to the other one that have collisions with the nucleus. Orbits 1, 3, 5, 7 belong to the family of stable PO and orbits 2, 4, 6 belong to the family of unstable PO, and all of them are EC-orbits. The stable periodic orbit labeled by 1 is the first one to collide with the nucleus as C decreases. This orbit is precisely the periodic 6-EC orbit of the family α_6 which has an initial angle $\theta_0 = \pi/2$. Similarly orbit labeled by 7 is the last one to collide with the nucleus as C decreases, and it belongs to family β_6 which has an initial angle $\theta_0 = 0$ (mod π). Orbits 1 and 7 do not belong to B_6^- whereas orbits 2, 3, 4, 5 and 6 do.

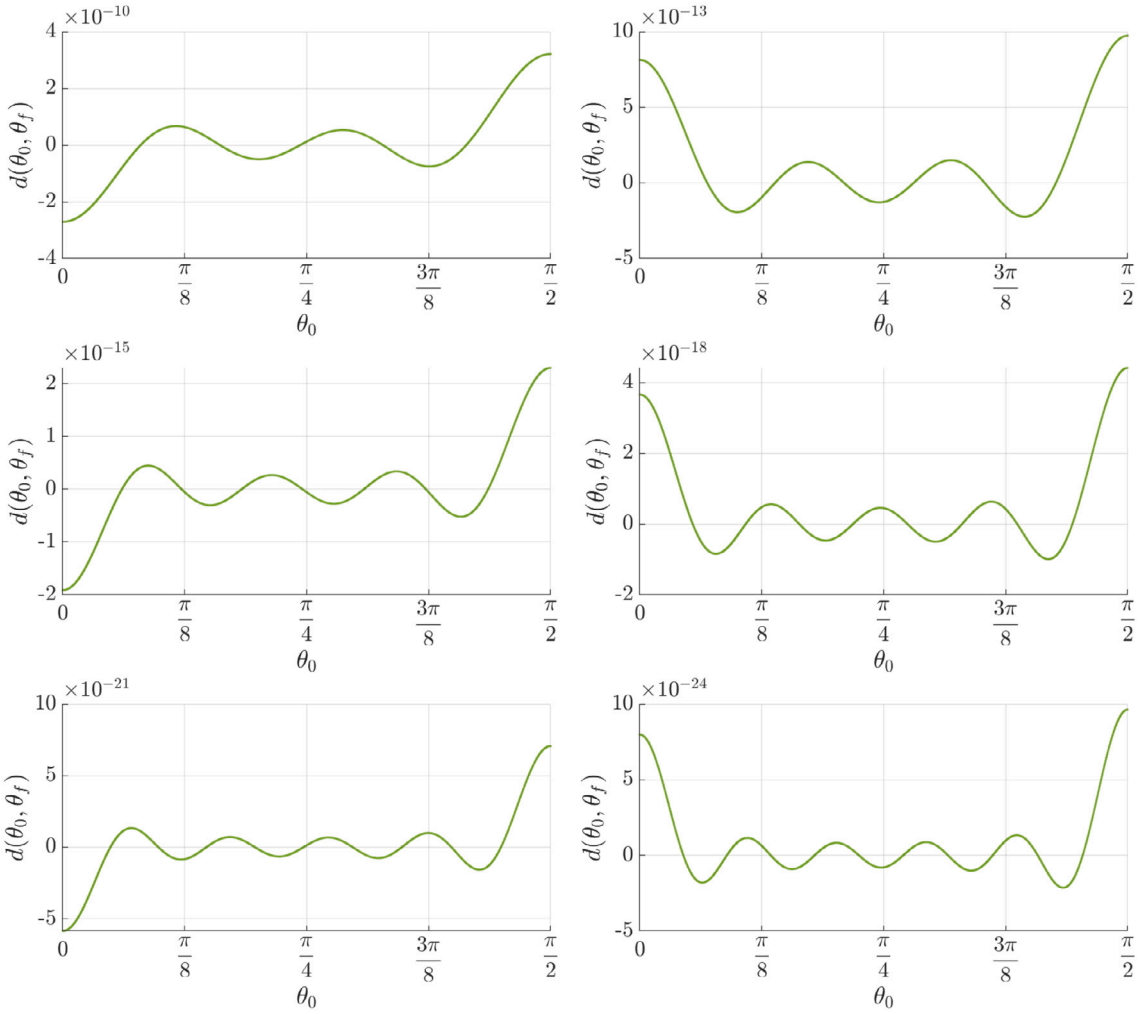

Fig. 9. $d(\theta_0, \theta_f)$ of the orbits of B_n^- for $K = 0.1$ and $n = 6, 7, 8, 9, 10, 11$ (from left to right and top to bottom).

Notice that whereas orbits 1 and 7 describe six petals and start and end at collision (and there are no intermediate collisions along the trajectory), this does not happen for orbits 2, 3, 4, 5 and 6. If we focus on the branch B_6^-, orbit 2 ejects, describes five petals, collides, ejects and describes one more petal and collides, completing six petals. We say that it is a 6-EC orbit of type $5 + 1$. Similarly orbit 3 ejects, describes four petals, collides, ejects, describes two petals and collides. So it is a 6-EC orbit of type $4 + 2$. Similarly orbit 4 is of type $3 + 3$, orbit 5 of type $2 + 4$ and orbit 6 of type $1 + 5$. See Fig. 10 where the actual path along the trajectory can be followed by the green numbering along the petals. Orbits 2, 3, 4, 5 and 6 belong to the branch B_6^- and each one has an initial value of θ_0, say θ_0^-. As previously remarked, there exists the corresponding value $\theta_0^+ = \pi - \theta_0^-$ that provides the initial angle for the same orbit but now belonging to the branch B_6^+ and with a different trajectory (that is the same orbit – as a set of points – but differently described). In Fig. 10 the trajectory can be followed by the purple numbering.

It is interesting to focus, just for a while, on the two families of PO (not EC orbits in general) and their relation with the EC orbits. Concerning the stability character of the orbits of the family of unstable/stable PO, we have obtained a very mild behavior. More precisely, we have computed the eigenvalues of the monodromy matrix for each periodic orbit, which are $\lambda_1 = 1$, $\lambda_2 = 1$, $\lambda_3 = \lambda$, $\lambda_4 = 1/\lambda$. For $K = 0.1$ and $n = 6$ and for the stable PO, the imaginary part of λ_3 is of order $1.e - 5$, similarly the same order is obtained for the difference from 1 of $\lambda_3 \in \mathbb{R}$ when taking the unstable PO. Such quantity increases with K but decreases when increasing n.

Surrounding each of these stable POs, we have a family of tori. This foliation of tori has a rotation number very close to 0 due to the fact that the imaginary part associated with the pair of complex eigenvalues of the monodromy matrix of the stable PO is very small. Thus, fixed a value of C, we have that the two EC orbits (belonging to B_n^- and B_n^+ respectively) either consist of these two POs (when $d = 0$) or are part of this foliation of tori that is invariant around the stable PO. This can be observed in Fig. 11, where we consider $K = 1$ and the Poincaré section $\Sigma = \{u = 0, u' > 0\}$. In the figure we take $C = 3.5$. We plot, first, the intersection of the two periodic orbits (which are not EC orbits), one which is stable (in blue) and one unstable (in red). Second, we plot in black the first 50000 intersections of the EC orbit belonging to B_6^+ with Σ. We remark that although it is a 6-EC orbit (in particular such intersection points contain two points belonging to the vertical line $v = 0$), since it is not periodic, the trajectory we go on and on (along time) describing (typically) a quasiperiodic orbit. We can see (more clearly in the zoom on the right), that this 6-EC is part of a torus around the stable PO. Finally, note that not all the EC orbits with $d \neq 0$ will be quasiperiodic, since, as it is well known, there will be resonances in the family of tori and therefore some of them will be POs with very long periods (recall that the imaginary part is very small).

Thus, in general, given n, the behavior of the first bifurcation of family α_n, is as follows: there exists a bifurcated family B_n (composed by the branches B_n^- and B_n^+) for $\theta_0 \in [0, \pi]$. Such bifurcation (where the two branches emerge) does not take place at $\theta_0 = \pi/2$ and the branches do not

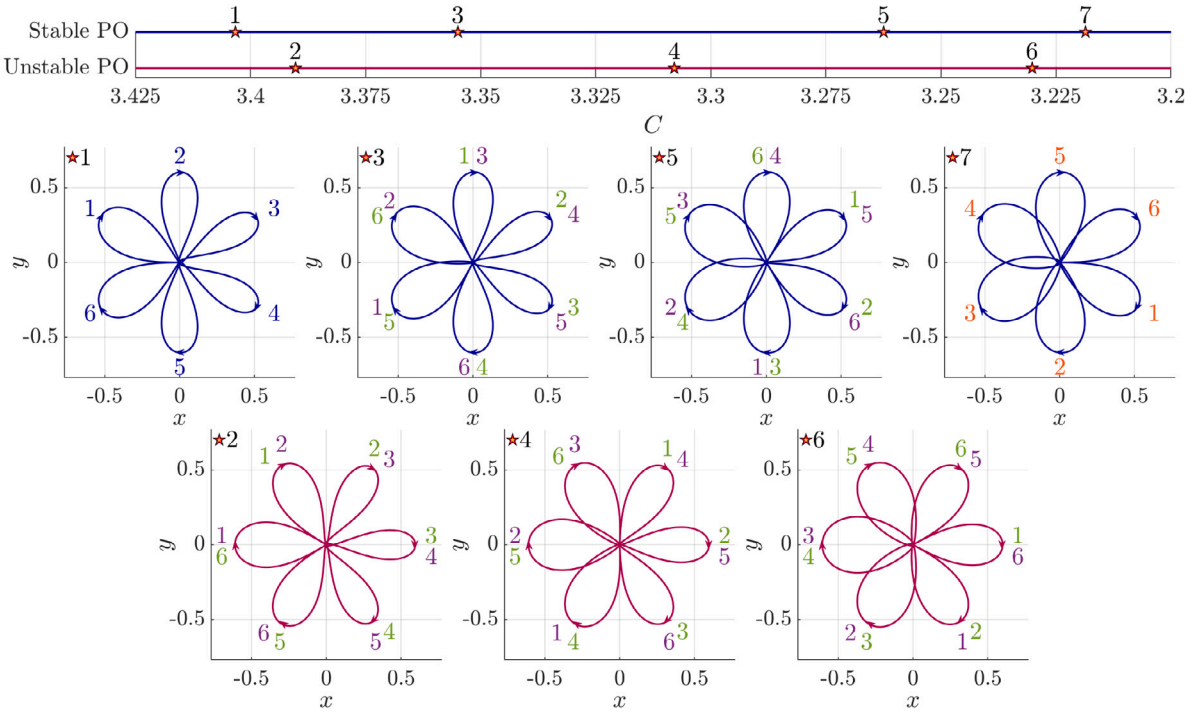

Fig. 10. Evolution of the collisions of the periodic orbits (PO) related with the bifurcation family B_6 for $K = 0.1$. Top: Values of C at which the seven collisions associated with the POs occur. Bottom: Trajectories of the POs with collisions. The numbers indicate the order in which the loops are traversed, and the color of the numbers indicates the family of 6-EC orbits to which they belong: blue for α_6, green for B_6^-, purple for B_6^- and red for β_6. In particular we have that the trajectory 1 belongs to the family α_6, the trajectories 2–6 belong to the families B_6^- and B_6^+ and the trajectory 7 belongs to β_6.

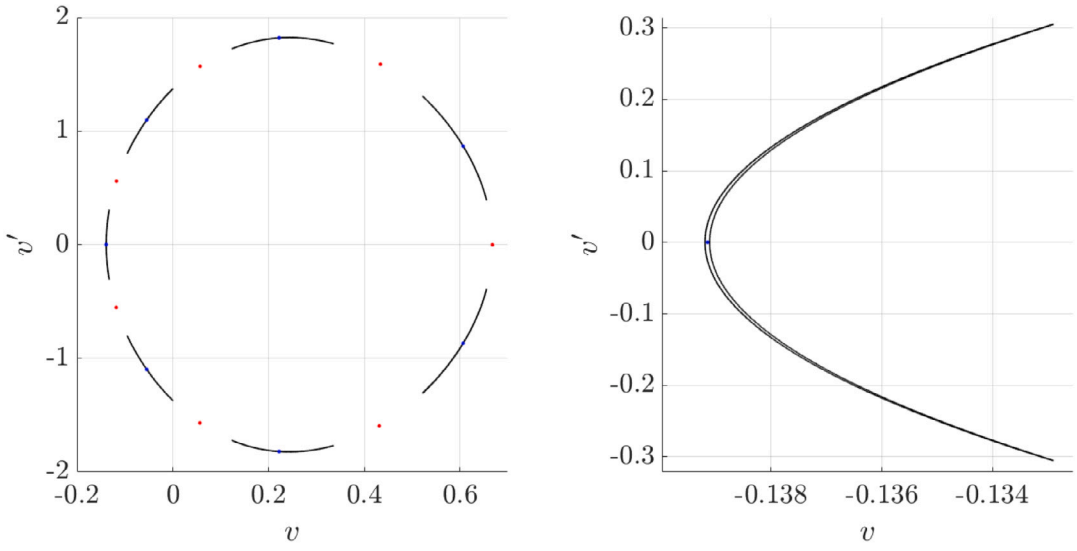

Fig. 11. Left: Intersection with $\Sigma = \{u = 0, u' > 0\}$ of the stable periodic orbit (blue) and the unstable one (red) that have 6 relative maximums in the distance from the first primary for $K = 1$ and $C = 3.5$. In black the first 50 000 intersections of the 6-EC orbit belonging to the B_6^+ with this value of C. Right: Zoom.

terminate at $\theta_0 = 0 \pmod{\pi}$ but with respective values very close to them. There exist two families of self-symmetric PO (one of stable PO and one of unstable PO) which contain (varying C) $n+1$ self-symmetric periodic orbits with collisions, say $k = 1, \dots, n+1$. The first periodic n-EC orbit ($k = 1$) is the one belonging to the family of stable PO and is the one belonging to family α_n for $\theta_0 = \pi/2$, but this orbit does not belong to the bifurcated branches; the $(n+1)$th one ($k = n+1$) belongs to the family of stable (unstable) PO for n even (odd) and belongs to family β_n for $\theta_0 = 0 \pmod{\pi}$, but this orbit does not belong to the bifurcated branches. Focusing on the branch B_n^-, only $n-1$ ($k = 2, \dots, n$) of the n-EC orbits are periodic. For $k = 2, \dots, n$, each periodic n-EC orbit has two collisions along the trajectory describing n petals. If k is even (odd), the corresponding PO belongs to the family of unstable (stable) PO. Actually these periodic n-EC orbits are the same ones for both branches B_n^- and B_n^+.

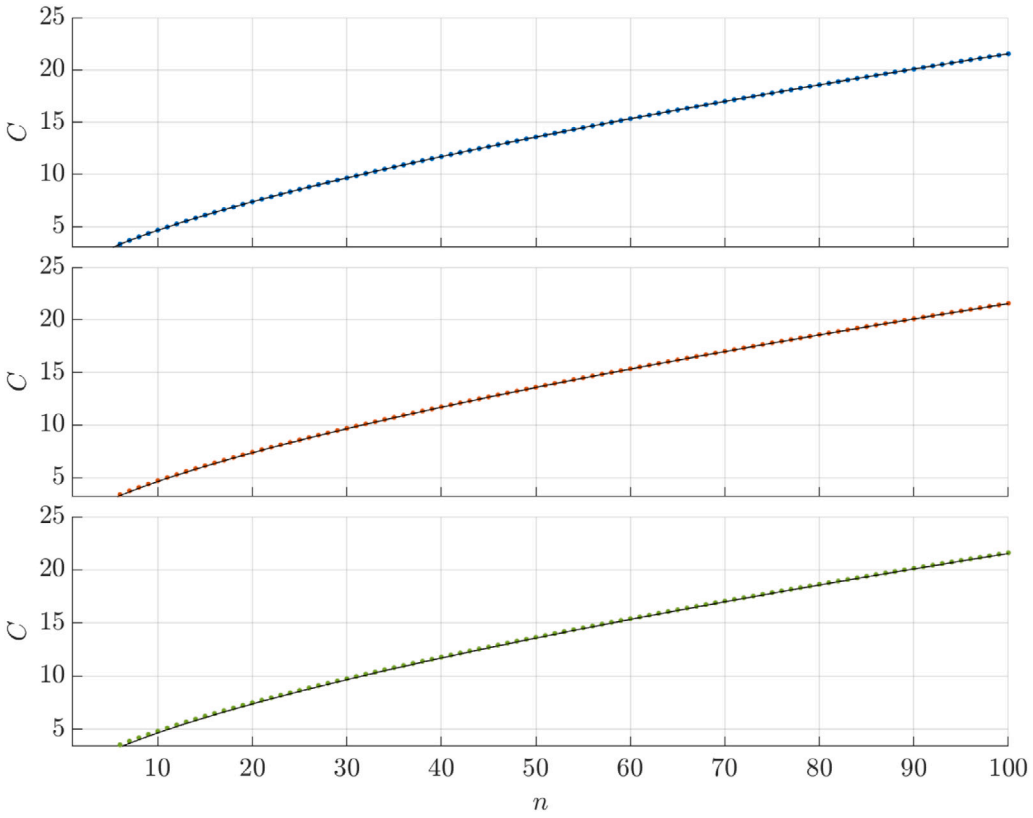

Fig. 12. The dots correspond to the values of $\hat{C}(K,n)$ for $K = 0.01$, $K = 0.1$ and $K = 0.2$ (from top to bottom) for $C \geq C_{L_1}(K)$. The continuous black curve is $n^{2/3}$.

4.3. Fitting the value of $\hat{L}$

Let us recall that in the proof of Theorem 1 the relation $C = Ln^{2/3}$ provides an explicit expression of the value of C as a function of n, such that there exist two n-ECO, for that value of C fixed big enough, and the implicit function theorem can be applied. Our next goal is to compute numerically, for a fixed value of $K > 0$ and $n \geq 1$, the (first) *limit* value $\hat{C}$ for which the first bifurcation appears, so that for $C > \hat{C}$ there exist only two ECO.

The method used consists in taking an interval $I = [C_a, C_b]$ of values of C, and for each $C \in I$, (starting at C_b) we vary $\theta_0 \in [0, \pi)$ and find the two specific values corresponding to the two expected n-EC orbits. As we decrease C, we find a value of $C \in I$ such that more than two n-EC orbits exist, which means that new families have bifurcated. Then, we refine the value of C where the bifurcation appears. That is precisely the specific value of $\hat{C}$. We show in Fig. 12 the results obtained for n ranging from 6 to 100, and the particular values of $K = 0.01$, 0.1 and 0.2, using different colors. We have considered $C \geq C_{L_1}$, which implies that only the cases $n \geq 6$ are explored (for $n = 1, \ldots, 5$, the value of C for which the first bifurcation appears is less than C_{L_1}).

Moreover we want an analytical expression for a good fitting of $\hat{C}$ depending on n. Theorem 1 predicts $\hat{C} = \hat{L}n^{2/3}$. In Fig. 12 we have also plotted the curve $\hat{C} = n^{2/3}$ as a continuous black curve. At first glance, we remark the good fitting taking $\hat{C} = \hat{L}n^{2/3}$ with the value $\hat{L} = 1$. In order to check such a fitting value of $\hat{L} = 1$, we have also computed the quotient $\hat{C}(K,n)/n^{2/3}$ in Fig. 13 varying n from 3 to 100 and for the same values of K. We observe that the smaller the value of K and the bigger the value of n, the better the fitting becomes.

Let us somewhat explain the reason for the fitting expression $\hat{C} = n^{2/3}$, which is precisely related to the periodicity. For any value of K and n let us consider the first bifurcating orbit, that is the n-EC orbit that we have observed that occurs at θ_0 very close to $\pi/2$. We notice from the computations that the first bifurcation takes place for a value of $C = \hat{C}$ such that the n-EC orbit is not periodic but very close to a periodic n-EC orbit (belonging to family α_n) which is periodic with period, in ordinary time t, very close to 2π.

We remark that 2π is precisely the rotation period of the rotating (synodical) system.

Now taking an order zero approximation (in K) for the ordinary time t in formula (32), with $t = 2\pi$, and the time $\mathcal{T}$ to reach the nth minimum in distance to the origin approximately as $\mathcal{T}_0^* = \pi$ (see (39)), we obtain

$$2\pi = 2\pi\varepsilon^3$$

so, $1 = \varepsilon^3$ or equivalently since $\varepsilon = 1/\sqrt{L}$, we get $L = \hat{L} = 1$.

We also want to remark that in this argument we are taking as ordinary time t, the one given by formula (32) and we are skipping the term $\mathcal{T}_1^*$ (see (39)) as well. From the expression of $\mathcal{T}_1^*$, we observe that K appears in the numerator, n in the denominator, so the fitting would become better (worse) as far as K decreases (increases) and n increases (decreases), with accordance to the behavior observed in Figs. 12 and 13.

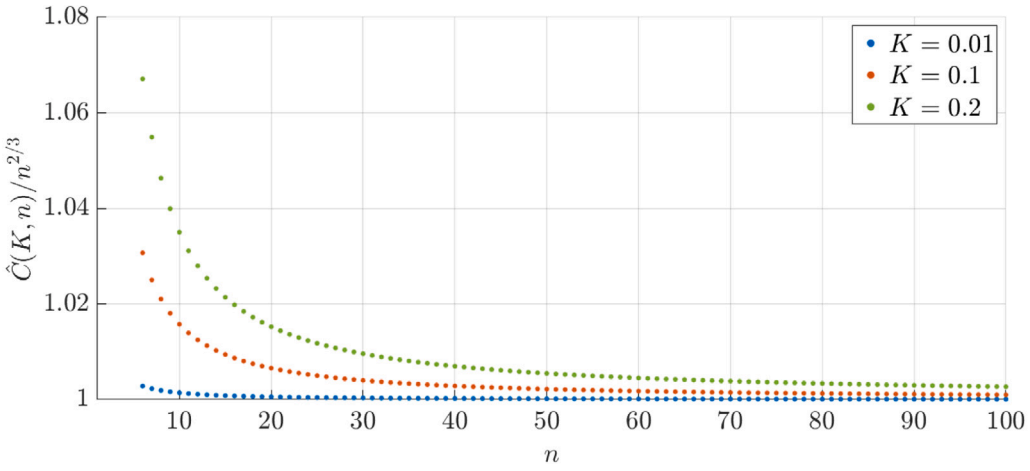

Fig. 13. Values of $\hat{C}(K,n)/n^{2/3}$ for $K = 0.01$, $K = 0.1$ and $K = 0.2$.

5. A sequence of bifurcations

The *first* bifurcation described so far appears for any value of n. See Fig. 7. However, as n increases, new bifurcations appear. See Fig. 14 where the first and second bifurcations are clearly seen for $K = 0.1$ and $n = 11, 12, 13, 14, 15, 16$.

The same kind of mechanism, discussed for the first bifurcation, applies for the subsequent bifurcations, that is, along the continuation of the main families α_n and β_n alternatively, each time that $\theta_0 = \pi/2$, the corresponding n-EC orbit is periodic with a period, in ordinary time t, very close to $2\pi p$, for $p = 1, 2, 3, \ldots$ (decreasing C). For n fixed, there appears a bifurcating family for θ_0 very close to, but different from, $\theta_0 = \pi/2$, at a particular value of C, say C_p. Thus we obtain in a successive way a sequence of values $C = C_p$ where the bifurcation occurs. For each p, the bifurcating family starts at C_p, exists for all $\theta_0 \in [0, \pi]$, giving rise to two branches in a small range of values of C. Such branches collapse at $\theta_0 = 0$ very close to 0 (mod π), that is, at a value of C different from, but very close to, the value of C of the periodic n-EC orbit of the family α_n or β_n accordingly. See Fig. 14.

We compute numerically the sequence of values of C_p, $p = 1, \ldots, 10$ and $n = 6, \ldots, 100$ for $K = 0.1$. They are shown in Fig. 15. We also plot the fitting curves $C_p(n) = (n/p)^{2/3}$, which indeed fit quite well the computed values C_p. The argument to achieve this expression is the same as in Section 4.3. However, now the successive bifurcations appear for values of θ_0 very close (but different) from $\pi/2$ and the n-EC bifurcating orbit is very close to the n-EC periodic orbit belonging to α_n or β_n with period in t very close to $2\pi p$ (that is, every p rotating periods), whereas the time from ejection to collision remains very close to $\mathcal{T}_0^* = \pi$. Therefore the expression (32) (taken as an approximation) now becomes

$$2\pi p = 2\pi\varepsilon^3$$

so $p = \varepsilon^3$ or, equivalently, $L = p^{-2/3}$ and the corresponding fitting curve becomes $C_p(n) = p^{-2/3}n^{2/3} = (n/p)^{2/3}$.

Again the smaller the value of K and the bigger the value of n, the better the fitting becomes.

5.1. Overlapping of families

We have seen in the previous Section that the successive bifurcations take place for values of θ_0 very close to $\pi/2$, at n-EC orbits close to the periodic n-EC orbits belonging to families α_n and β_n. Similarly the collapse of branches take place at θ_0 very close to π.

Now let us explain *a double* overlapping phenomena concerning the families of n-EC orbits and the bifurcated families.

Notice a first effect of overlapping in Fig. 16. The families α_6, β_{12}, α_{18}, β_{24} and α_{30} (in general $\alpha_{6(2k-1)}$ and $\beta_{6(2k)}$, for $k \geq 1$) cross along their way the same point at $\theta_0 = \pi/2$. The same basic periodic 6-EC orbit is described 2, 3, 4 and 5 times (in general $2k-1$ and $2k$ times) respectively regarded as an orbit of the corresponding family. The same kind of overlapping takes place for families β_6, α_{12}, β_{18}, α_{24} and β_{30} at $\theta_0 = \pi$. We have shown this first effect of overlapping for $n = 6$, but of course it also applies for any value of n.

Let us concentrate on the bifurcated families. From now on, we define the label α_n^i as the ith intersection of family α_n with $\theta_0 = 0$ (mod $\pi/2$). Similarly for β_n^i. First, we introduce some notation: we denote by B_n^i the ith bifurcated family of n-EC orbits, similarly $B_n^{i\pm}$ the corresponding branches (and for $i = 1$, we simply write B_n, $B_n^{\pm}$). Moreover we say that a bifurcated family is *basic* if it is labeled as B_q^p with $\gcd(p, q) = 1$.

The same kind of properties observed for the bifurcating families at the first bifurcation do apply in general:

(i) The families B_{iq}^{ip} are very close to each other in the sense that $\frac{iq}{ip} = \frac{q}{p}$, but they bifurcate (and end) at different values of θ_0 very close to $\pi/2$ (and π). In Fig. 16, the bifurcated families B_6, B_{12}^2, B_{18}^3, B_{24}^4 and B_{30}^5 are shown. They are all born at a (different) corresponding value of θ_0 very close to $\theta_0 = \pi/2$ and collapse at a different (associated) value of θ_0 close to $\theta_0 = \pi$. However they are so close to each other that they cannot be distinguished in the figure.

(ii) Regarding the relation between periodic orbits and the orbits belonging to the bifurcated families, we obtain the same kind of behavior as explained in the previous Section: the family B_q^p, with $\gcd(p, q) = 1$, has $q-1$ periodic q-EC orbits, called *basic* orbits. The corresponding trajectories describe q petals doing p rounds (around the origin in synodical coordinates (x, y)). Remarkably, these periodic EC orbits are particular members of one or other family of the two existing families of symmetric periodic orbits – in general without collisions – (alternating a stable periodic orbit and an unstable periodic one).

Moreover, the families B_{iq}^{ip} are different but coincident in these particular $q-1$ periodic q-EC orbits. This is precisely the second peculiar overlapping phenomenon. Each such orbit belonging to B_{iq}^{ip} is the same orbit as the basic one but described i times. To illustrate the existence of

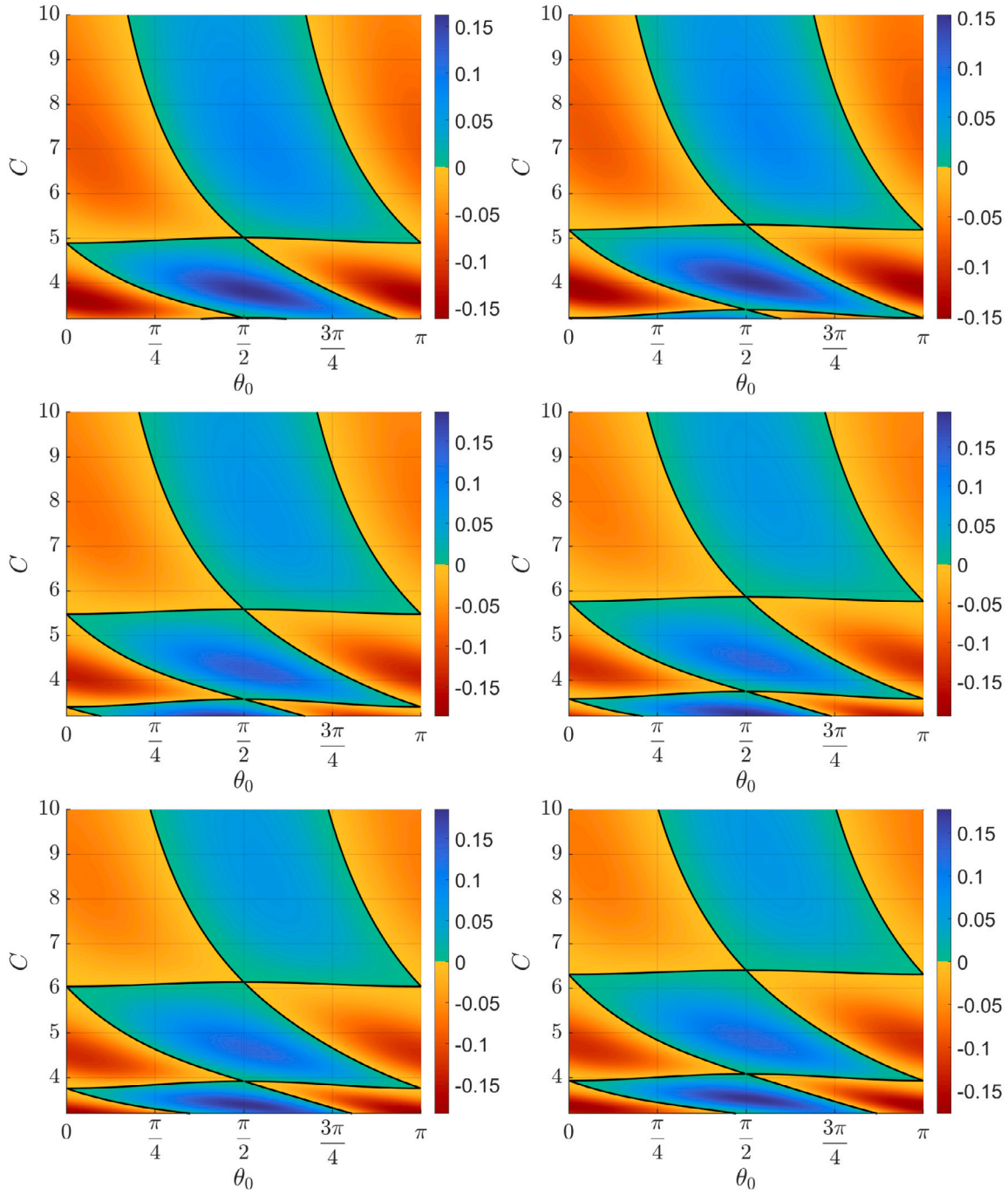

Fig. 14. Value of the angular momentum $K = 0.1$, $n = 11, 12, 13, 14, 15, 16$.

(and coincidence at) these $q-1$ periodic q-EC orbits belonging to family B_{iq}^{ip}, in Fig. 17 we show the distance $d(\theta_0, \theta_f)$ for the branches B_6^-, B_{12}^{2-}, B_{18}^{3-}, B_{24}^{4-} and B_{30}^{5-}. The $q-1$ periodic orbits correspond to the zeros of $d(\theta_0, \theta_f)$, which are coincident for the different branches.

(iii) The ith bifurcation B_n^i is born from the main family α_n very close to α_n^i if i is odd, or from the main family β_n very close to β_n^i if i is even. Similarly for the collapse of the bifurcating branches. See Fig. 18.

Another way to explain this overlapping of families is shown in Fig. 18. Rather than focusing on the bifurcating families (branches), let us concentrate on the successive intersections of families α_n and β_n with $\theta_0 = \pi/2$, where periodic n-EC take place. Recall that α_n^i (β_n^i) stands for the ith intersection of family α_n with $\theta_0 = 0 \pmod{\pi/2}$. The same label will also be used for the associated periodic n-EC orbit (of the family) which is which describes n petals doing i rounds. We obtain:

$$\text{for } \alpha_n^i: \begin{cases} \theta_0 = 0 \pmod{\pi}, & i \text{ even}, \\ \theta_0 = \pi/2 \pmod{\pi}, & i \text{ odd}, \end{cases} \qquad \text{for } \beta_n^i: \begin{cases} \theta_0 = 0 \pmod{\pi}, & i \text{ odd}, \\ \theta_0 = \pi/2 \pmod{\pi}, & i \text{ even}. \end{cases}$$

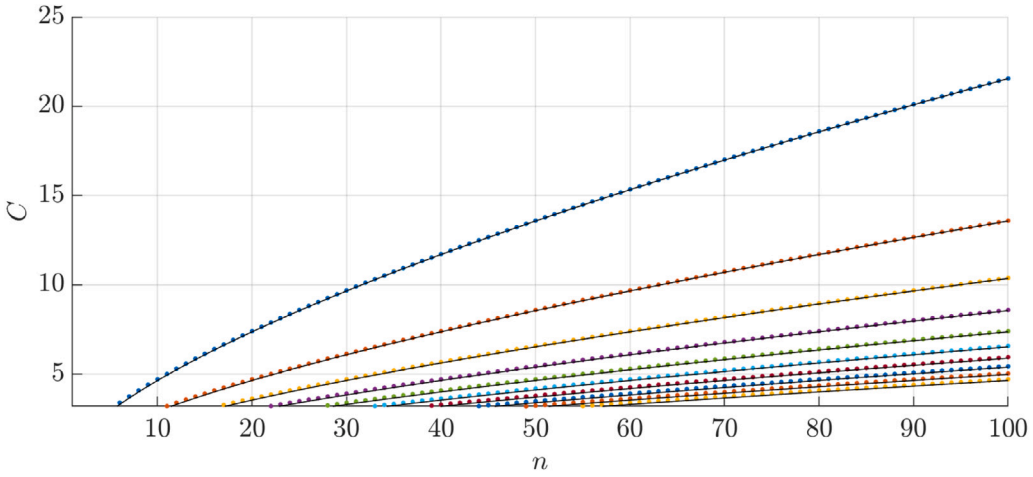

Fig. 15. $K = 0.1$. The dots correspond to the first 10 bifurcation values of C_p (assuming $C \geq C_{L_1}(K)$). The black continuous curves correspond to the fitting curves $(n/p)^{2/3}$ with $p = 1, \ldots, 10$.

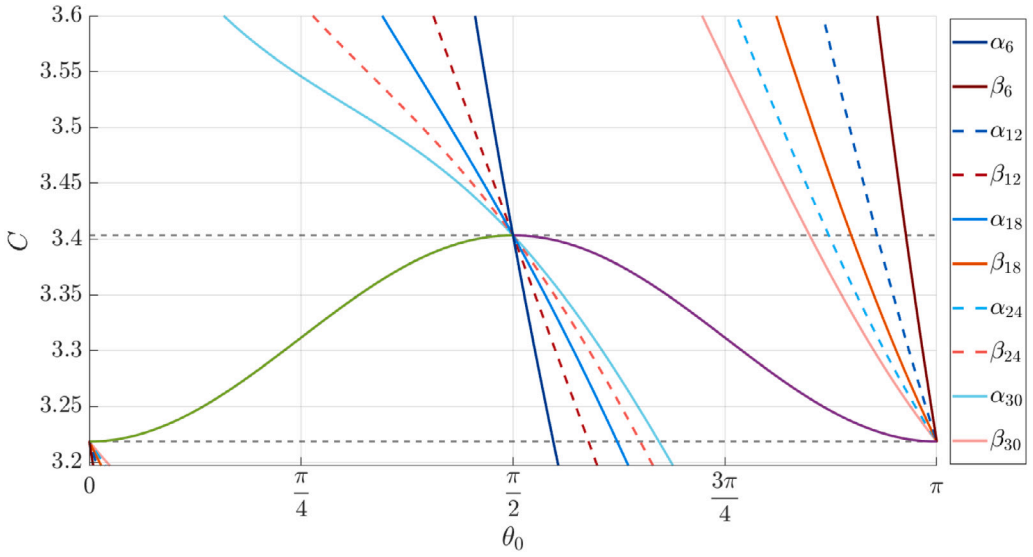

Fig. 16. $K = 0.1$. Overlapping of families. The bifurcated families B_6, B_{12}^2, B_{18}^3, B_{24}^4 and B_{30}^5 (in green and purple) are born all very close to $\theta_0 = \pi/2$ and collapse close to $\theta_0 = 0$.

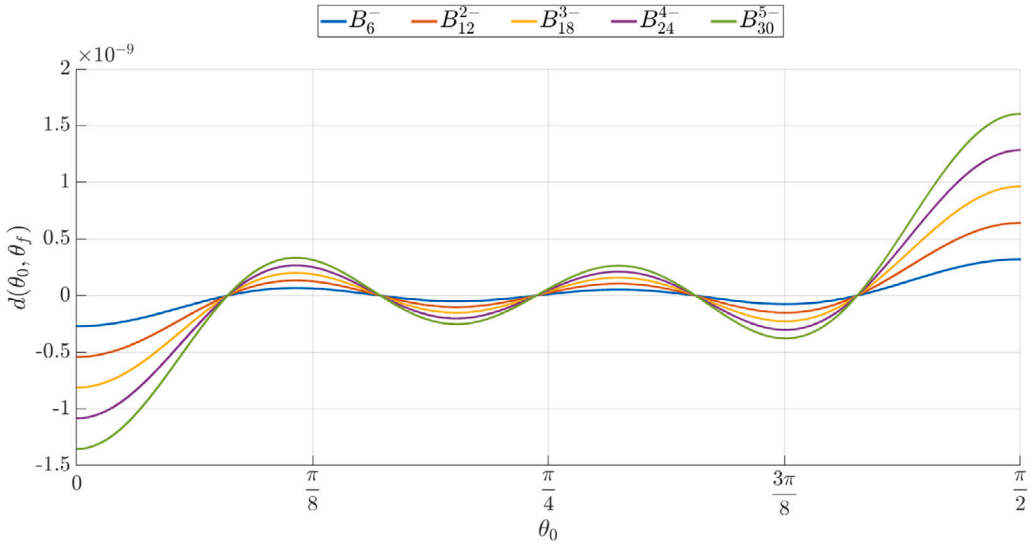

Fig. 17. $d(\theta_0, \theta_f)$ of the orbits of B_{6j}^{j-} for $K = 0.1$ and $j = 1, \ldots, 5$.

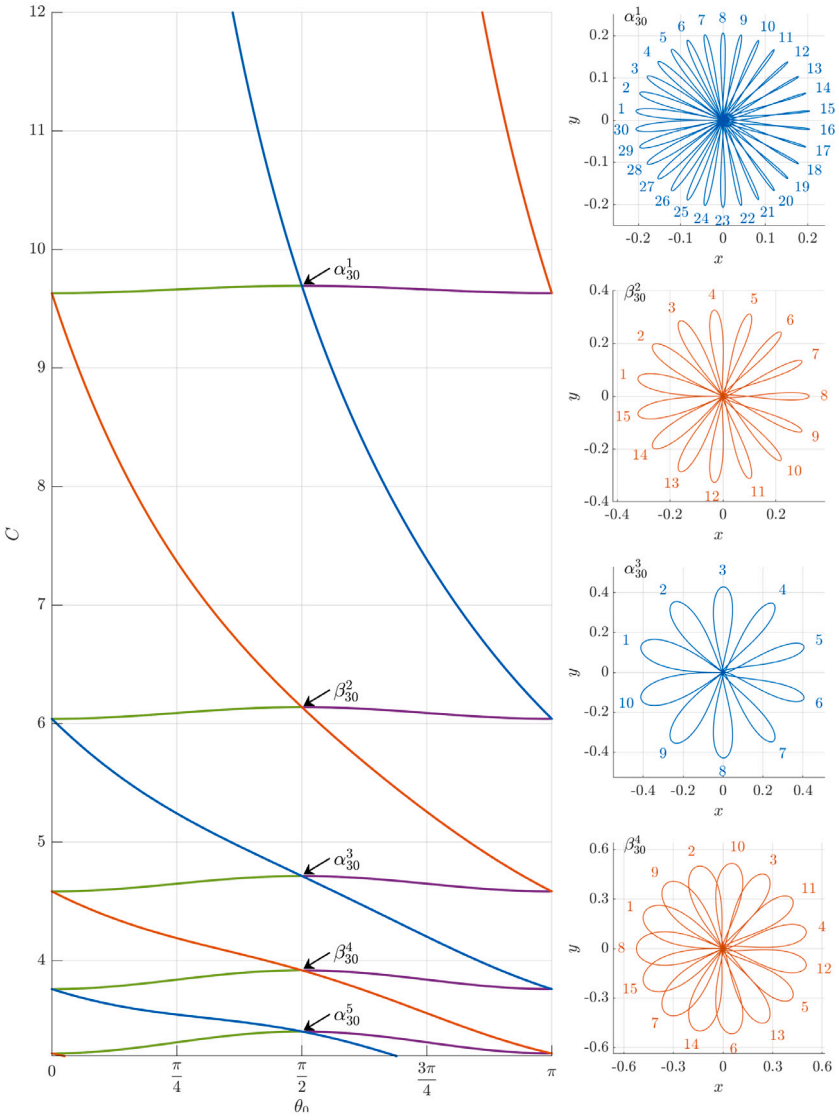

Fig. 18. $K = 0.1$ and $n = 30$. Left. Continuation of families α_{30} and β_{30} and the appearing bifurcations when decreasing C. Right. The periodic EC orbits at $\theta_0 = \pi/2$.

Moreover, given α^p_q with $\gcd(p, q) = 1$ (that is, a basic periodic EC orbit describing q petals doing p rounds), all the points labeled $\alpha^{(2k+1)p}_{(2k+1)q}$ and β^{2kp}_{2kq} coincide at α^p_q (similarly interchanging α and β), and the corresponding trajectory is the same one as the basic orbit simply described the number of times given by the multiplicity.

Let us show that property in Fig. 18. The main two families for values of C decreasing from $C = 12$ are the families α_{30} (the blue curve on the figure) and β_{30} (the red curve). Let us denote by α^1_{30}, β^2_{30}, α^3_{30}, β^4_{30}, α^5_{30} the corresponding points in the Figure at $\theta_0 = \pi/2$ when decreasing C. We see the first intersection of family α_{30} with $\theta_0 = \pi/2$ at point α^1_{30} (and we notice the bifurcation of two branches of 30-EC orbits that emerge – collapse – for θ_0 close to $\pi/2$ –π–). We show this periodic 30-EC orbit α^1_{30} in Fig. 18 top right. The trajectory describes 30 petals along one round, and, since it is the first intersection of family α_{30} with $\theta_0 = \pi/2$, this implies that the time t to describe the 30-EC orbit (from ejection to collision) is close to 2π.

Decreasing C, the family β_{30} crosses $\theta_0 = \pi/2$ at point β^2_{30}. Through this point there has been a previous intersection of family α_{15}, say at point α^1_{15}. In Fig. 18 right, we show the basic periodic 15-EC orbit α^1_{15} with 15 petals along one round and the time t to describe the 15-EC orbit is close to 2π, since it is the first intersection of family α_{15} with $\theta_0 = \pi/2$ as can be seen in Fig. 14. The same orbit is described twice regarded as the orbit β^2_{30} (thirty petals doing two rounds) belonging to family β_{30}.

Next, decreasing C, we see the family α_{30} which crosses $\theta_0 = \pi/2$ at point α^3_{30}. At this point families β_{20} and α_{10} have already crossed this point at β^2_{20} and α^1_{10} respectively. The basic periodic EC orbit corresponds to α^1_{10}, which is a 10-EC orbit (with ten petals along one round) and also can be regarded as an orbit described twice as an orbit of family β_{20} or an orbit described three times regarded as an orbit of family α_{30}. See Fig. 18 right. Notice that since the family α_{10} has the first intersection at α^1_{10} (see Fig. 7), the time t from ejection to collision is close to 2π.

Decreasing C, an analogous behavior takes place for the overlapping of families β_{30} and β_{15} at point $\beta^4_{30} = \beta^2_{15}$. Now, though, the basic orbit describes fifteen petals doing two rounds – recall the notation β^2_{15} – and the original time t spent along the 15-EC orbit from ejection to collision is close to $4\pi = 2 \cdot 2\pi$. We show the basic orbit in Fig. 18 right, where the numbering of the petals helps counting the number of rounds. The same orbit can bed regarded as β^4_{30} (i.e. thirty petals doing four rounds).

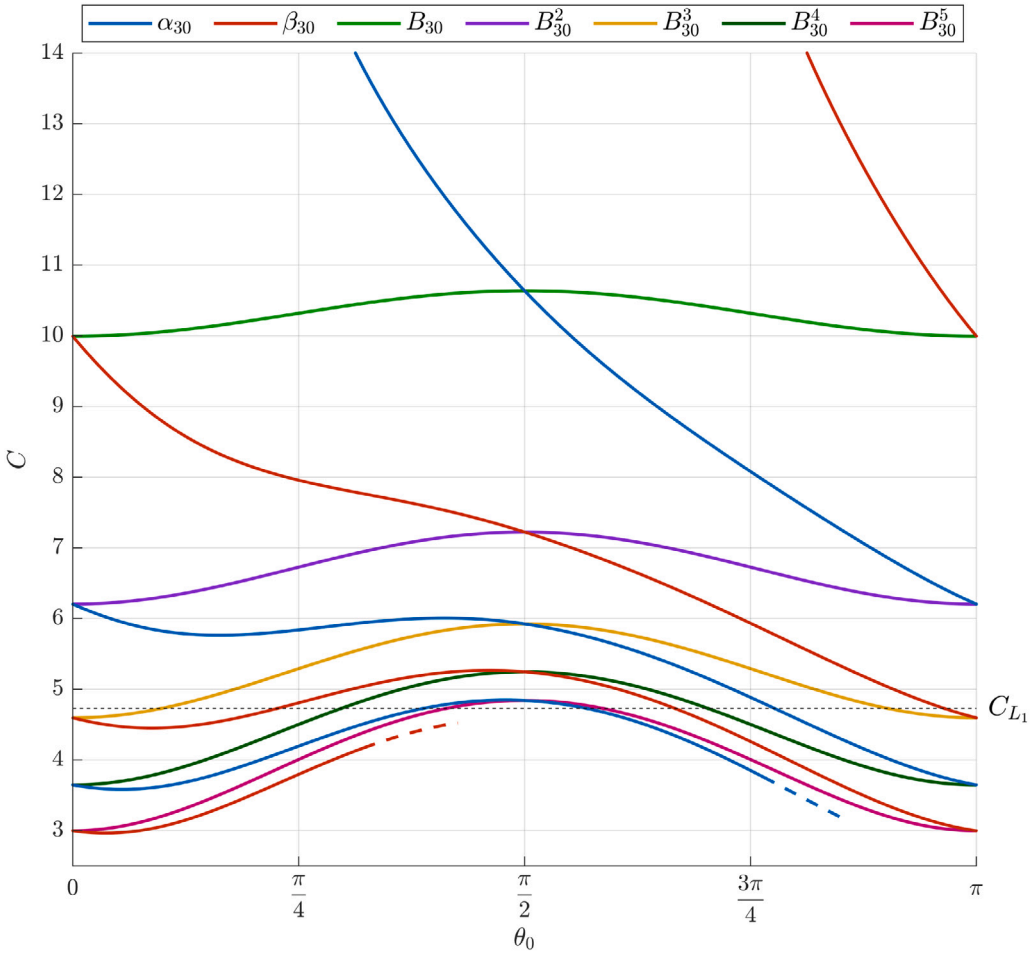

Fig. 19. $K = 1$ and $n = 30$. Continuation of families α_{30} and β_{30} and the appearing bifurcations when decreasing C.

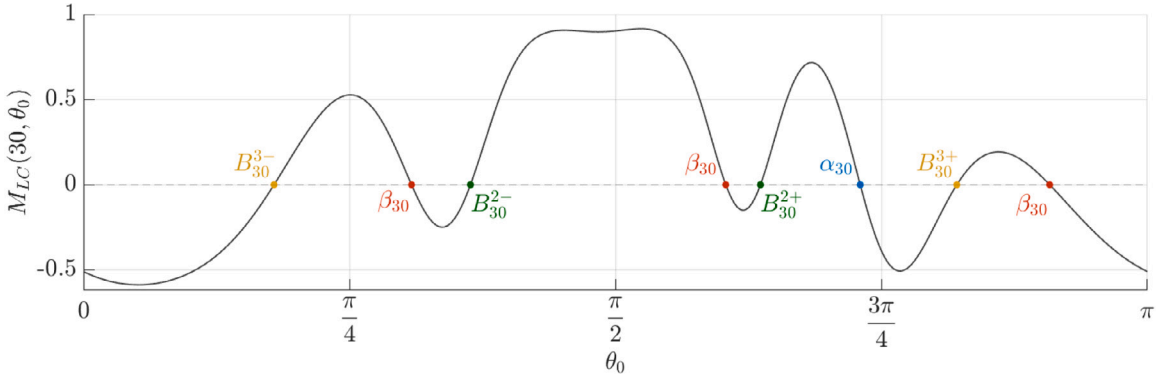

Fig. 20. $K = 1$, $n = 30$ and $C = 5$. Curve $M_{LC}(30, \theta_0)$. In colors the EC orbits and the labels of the families (branches) they belong to.

Decreasing C, similarly an overlapping of families α_{30} and α_6 occurs at point $\alpha_{30}^5 = \alpha_6^1$. The basic periodic 6-EC orbit (as an orbit of family α_6) describes six petals doing one round and the time from ejection to collision is close to 2π. The orbit is already shown in Fig. 8 top right. The same orbit can be regarded as α_{30}^5, that is describing thirty petals doing five rounds.

To conclude let us make the following two comments concerning the bifurcated families. The first observation is that, naturally, as we increase the value of n and decrease the value of C, more bifurcations appear. This is expected, as we have mentioned, since the value of C at which the pth bifurcation of the n-EC orbits occurs is close to $(n/p)^{2/3}$. The second one is that the range in C where each bifurcating family exists clearly depends on the parameters of the problem. More precisely, from the numerical simulations we infer that as $K > 0$ gets smaller the range in C where the bifurcated families exist is really thin. However, as $K > 0$ increases, this range increases and the bifurcated families are closer to each other. We show this phenomenon in Fig. 19 for $K = 1$, where we have followed the continuation of families α_{30} and β_{30} and the bifurcated families as well. Compare Figs. 18 and 19. We notice that, whereas for $K > 0$ small ($K = 0.1$ in Fig. 18) and for any value of C (in the figure), we obtain either two EC orbits (one belonging to each family α_{30} and β_{30}) or four EC orbits (two additional EC orbits that belong to a bifurcated family). However,

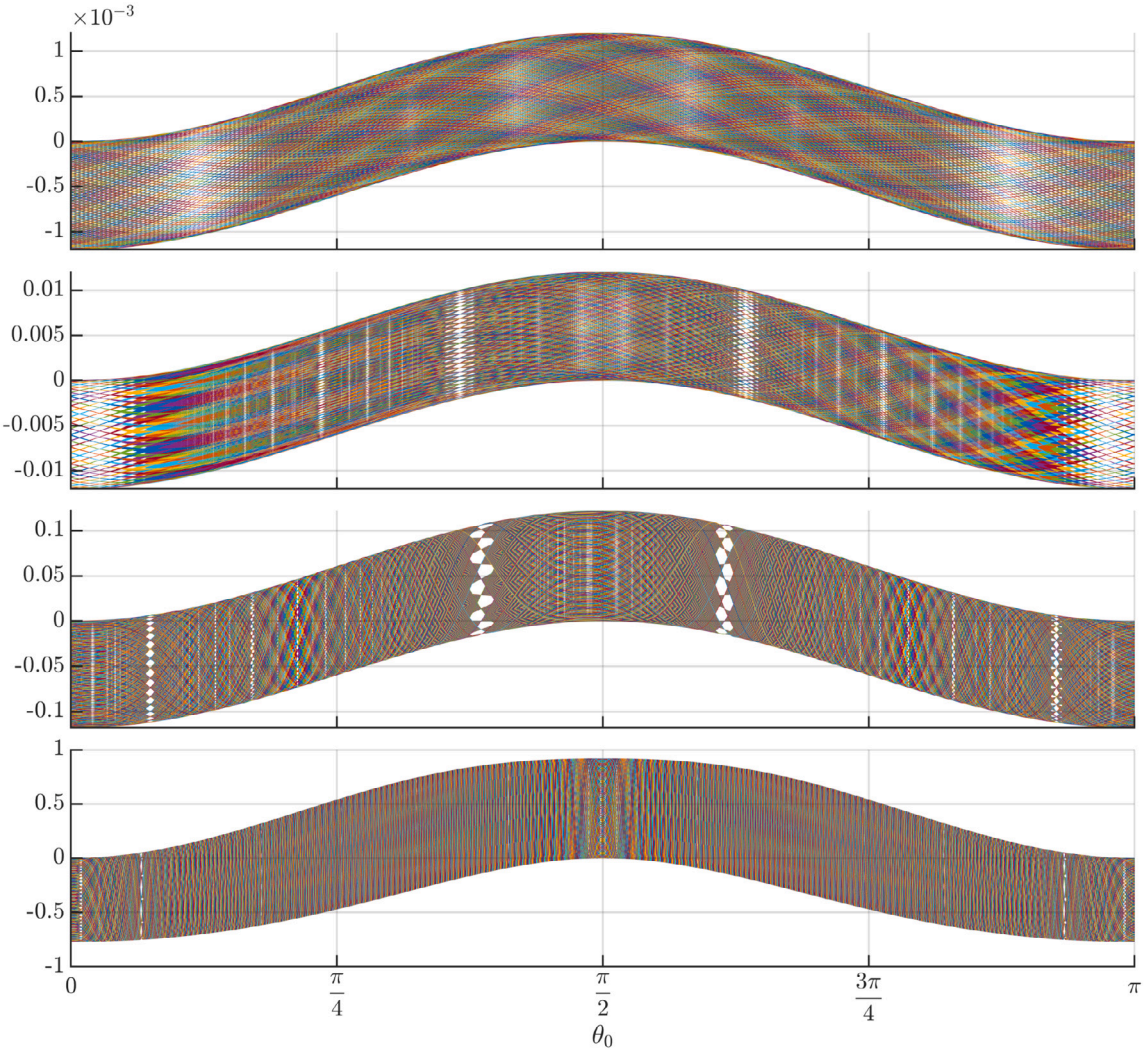

Fig. 21. Curves $M_{LC}(n,\theta_0)$ for $n = 1,\dots,1000$ for $C = 5$ and $K = 10^{-3}, 10^{-2}, 0.1, 1$ (from top to bottom).

as $K > 0$ increases, besides the fact that the bifurcated families exist on bigger ranges of values of C these families get close to each other, that is we observe an accumulation among the bifurcated families and the main families α_n and β_n. In this case, given a value of C, there may exist more than four EC orbits. We show this effect in Fig. 20, for $K = 1$, $n = 30$ and $C = 5$. We plot the curve $M_{LC}(30,\theta_0)$. We observe there exist eight intersection points with the horizontal axis ($M_{LC}(30,\theta_0) = 0$), which correspond to eight different EC orbits. We label each EC orbit by the label of the family (or branch) they belong to using the same color code as in Fig. 19.

5.2. Global behavior of the ejection orbits

The behavior of n-EC orbits can be easily observed when studying the global behavior of ejection orbits. As previously explained, the bifurcations of n-EC orbits that arise from the α_n and β_n families have a periodic or a quasi-periodic character. Since the families of periodic orbits associated with these bifurcations have a very weak character, we can globally detect the different n-EC orbits that exist for a particular value of C by observing the value of the angular momentum at successive crossings with the minimum, i.e., by studying $M_{LC}(n,\theta)$ for various values of n at the same time.

For example, in Fig. 21, we plot the curve $M_{LC}(n,\theta_0)$ for $n = 1,\dots,1000$ for $K = 10^{-3}, 10^{-2}, 0.1, 1$ and $C = 5$. From this figure one can note that the angular momentum value is clearly bounded. This is expected, as for values of $C \geq C_{L_1}$ the Hill region enforces the electron to have a bounded motion around the nucleus. Furthermore, it can also be noted that for certain values of θ_0, the value of $M_{LC}(n,\theta_0)$ accumulates around specific points. Such behavior is due to the fact that for these values of θ_0, we have an n-EC orbit (and other ejection orbits close to it) belonging to one of the EC bifurcation families. Note again that this behavior is due to the stability of the periodic orbits associated with the bifurcation.

This last observation can be seen in more detail in Fig. 22, which shows the case $K = 0.1$ and a zoom of it. In Fig. 22 top we also mark the ejection angles θ_0 associated with the two 11-EC orbits belonging to branches B_{11}^{-} and B_{11}^{+} and two 34-EC orbits belonging to branches B_{34}^{3-} and B_{34}^{3+}. In this top figure we also observe other accumulation points for M_{LC}, and if we focus in a particular range of θ_0 we can detect more (see Fig. 22 bottom). We remark that in Fig. 22 we only mark some of the θ_0 values of the EC orbits associated with the *basic* bifurcations $B_q^{p\pm}$ (where p and q are coprime), but close to them there are other n-EC orbits associated with the families $B_{qi}^{pi\pm}$ with $i \geq 2$. We emphasize that we only mark the most visible bifurcation families but it is clear that there are many more. So there appears a rich bifurcating structure of bifurcated EC orbits.

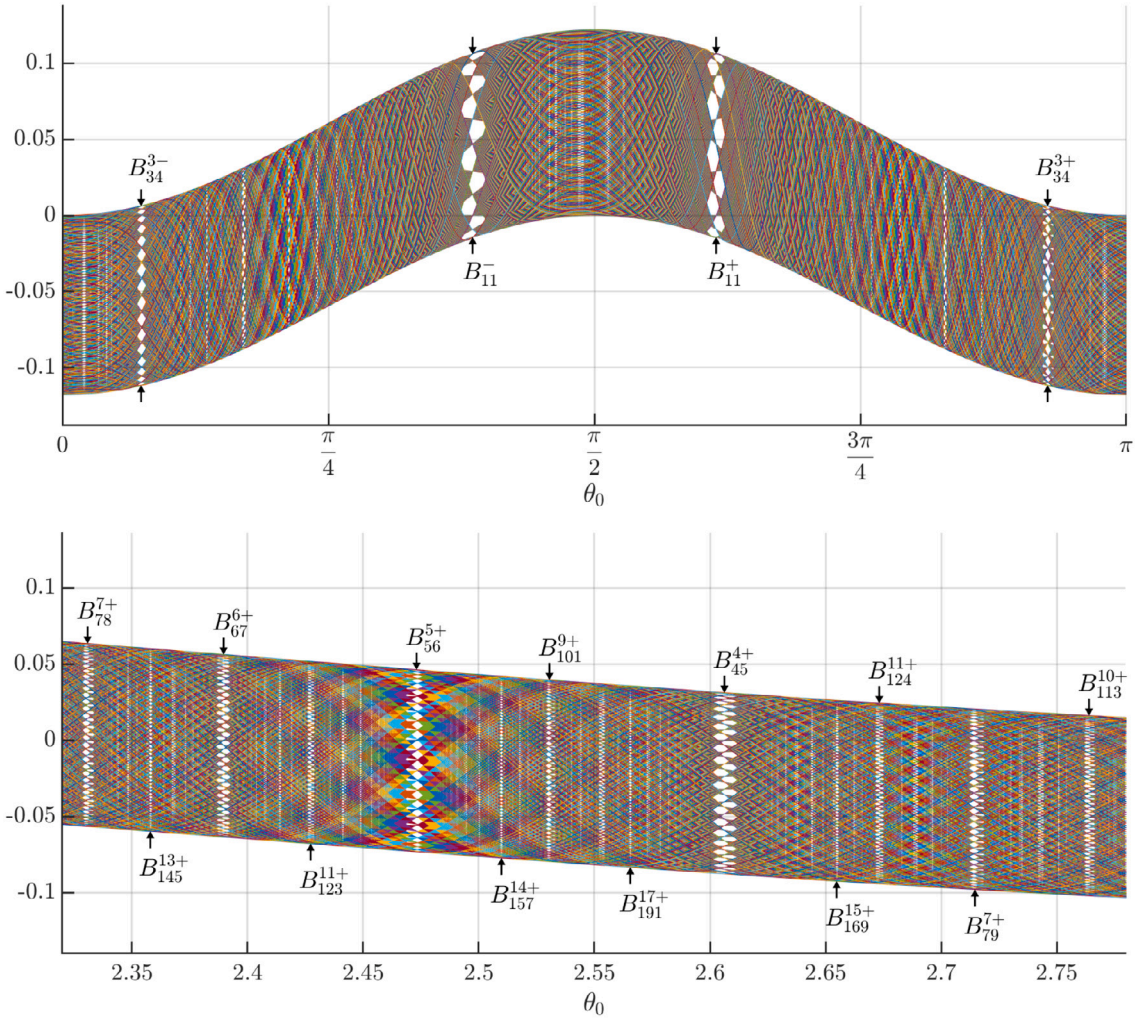

Fig. 22. $K = 0.1$. Curves $M_{LC}(n, \theta_0)$ for $n = 1, \ldots, 1000$ and $C = 5$. Zoom area. The label $B_q^{p\pm}$ plus an arrow stands for the θ_0 of an EC orbit belonging to such family.

CRediT authorship contribution statement

Esther Barrabés: Conceptualization, Investigation, Methodology, Software, Validation, Writing – original draft, Writing – review & editing. **Mercè Ollé:** Conceptualization, Investigation, Methodology, Software, Validation, Writing – original draft, Writing – review & editing. **Óscar Rodríguez:** Conceptualization, Investigation, Methodology, Software, Validation, Writing – original draft, Writing – review & editing.

Declaration of competing interest

The authors declare that they have no known competing financial interests or personal relationships that could have appeared to influence the work reported in this paper.

Data availability

Data will be made available on request.

Acknowledgments

This work is supported by the Spanish State Research Agency, through the Severo Ochoa and María de Maeztu Program for Centers and Units of Excellence in R&D (CEX2020-001084-M). The authors were also supported by the Spanish grant PID2021-123968NB-I00 (AEI/FEDER/UE).

Appendix A. Proof of Theorem 1

Recently, in [19], the authors prove the existence of, not two but, four families of n-EC orbits in the circular restricted three-body problem (RTBP). The proof of Theorem 1 follows similar arguments. Next, in order to be self contained, we present here the baseline of the proof, and place the more technical details to Appendix B for any interested reader.

The process of the proof is as follows. First, inspired in the change of variables applied in the RTBP, we introduce the following change of variables and time:

$$u = \frac{\sqrt{2}}{\sqrt{L}n^{1/3}}\,\mathcal{U}, \qquad v = \frac{\sqrt{2}}{\sqrt{L}n^{1/3}}\,\mathcal{V}, \qquad \mathcal{T} = \frac{2\sqrt{L}}{n^{2/3}}\,s, \qquad C = Ln^{2/3}. \tag{22}$$

Then, system (11) becomes

$$\begin{cases} \ddot{\mathcal{U}} = -n^2\mathcal{U} + 8\left(\mathcal{U}^2+\mathcal{V}^2\right)\dot{\mathcal{V}}\varepsilon^3 + 12\left(\mathcal{U}^2+\mathcal{V}^2\right)^2\mathcal{U}\varepsilon^6 - 8Kn^{2/3}\mathcal{U}^3\varepsilon^4, \\ \ddot{\mathcal{V}} = -n^2\mathcal{V} - 8\left(\mathcal{U}^2+\mathcal{V}^2\right)\dot{\mathcal{U}}\varepsilon^3 + 12\left(\mathcal{U}^2+\mathcal{V}^2\right)^2\mathcal{V}\varepsilon^6 + 8Kn^{2/3}\mathcal{V}^3\varepsilon^4, \end{cases} \tag{23}$$

where $\varepsilon = 1/\sqrt{L}$ and $\dot{} = \frac{d}{d\mathcal{T}}$. System (23) has the same properties as the ones described above for the system (11) in Levi-Civita regularization, since the change (22) consists simply in a rescaling of the variables and time. Notice that for C big enough, ε becomes a small parameter.

Next Lemma gives a situation in which Proposition 1 can be applied in the context of system (23).

Lemma 1. *If C is large enough and a solution of system (23) is in the interior of the bounded component of the Hill's region and located at a minimum in the distance to the origin, then $\dot{\mathcal{U}}^2 + \dot{\mathcal{V}}^2 \neq 0$.*

Proof. The proof is as follows. If $\mathcal{U} = \mathcal{V} = 0$, using the Jacobi integral (15) and the change (22), we have that $\dot{\mathcal{U}}^2 + \dot{\mathcal{V}}^2 = n^2 \neq 0$.

Suppose that $\mathcal{U}^2 + \mathcal{V}^2 > 0$ and $\dot{\mathcal{U}} = \dot{\mathcal{V}} = 0$. Then the solution is on the zero velocity curve inside the bounded component of the Hill's region and it cannot be at a minimum of the distance to the origin function. In fact, if it were at a minimum, its second derivative $\mathcal{U}\ddot{\mathcal{U}} + \mathcal{V}\ddot{\mathcal{V}}$ cannot be negative at this point. Using the equations of motion (23):

$$\mathcal{U}\ddot{\mathcal{U}} + \mathcal{V}\ddot{\mathcal{V}} = -n^2(\mathcal{U}^2+\mathcal{V}^2) - 8Kn^{2/3}(\mathcal{V}^4 - \mathcal{U}^4)\varepsilon^4 + 12(U^2+V^2)^3\varepsilon^6,$$

but this quantity is negative for ε small enough if $\mathcal{U}^2 + \mathcal{V}^2$ is not big, which contradicts the hypothesis. □

Let us introduce the vector notation $\boldsymbol{\mathcal{U}} = (\mathcal{U}, \mathcal{V}, \dot{\mathcal{U}}, \dot{\mathcal{V}})$. The system (23) can be written as

$$\dot{\boldsymbol{\mathcal{U}}} = \boldsymbol{\mathcal{F}}_0(\boldsymbol{\mathcal{U}}) + K\boldsymbol{\mathcal{F}}_1(\boldsymbol{\mathcal{U}}), \tag{24}$$

where

$$\boldsymbol{\mathcal{F}}_0(\boldsymbol{\mathcal{U}}) = \begin{pmatrix} \dot{\mathcal{U}} \\ \dot{\mathcal{V}} \\ -n^2\mathcal{U} + 8(\mathcal{U}^2+\mathcal{V}^2)\dot{\mathcal{V}}\varepsilon^3 + 12(\mathcal{U}^2+\mathcal{V}^2)^2\mathcal{U}\varepsilon^6 \\ -n^2\mathcal{V} - 8(\mathcal{U}^2+\mathcal{V}^2)\dot{\mathcal{U}}\varepsilon^3 + 12(\mathcal{U}^2+\mathcal{V}^2)^2\mathcal{V}\varepsilon^6 \end{pmatrix}, \quad \boldsymbol{\mathcal{F}}_1(\boldsymbol{\mathcal{U}}) = 8n^{2/3}\varepsilon^4 \begin{pmatrix} 0 \\ 0 \\ -\mathcal{U}^3 \\ \mathcal{V}^3 \end{pmatrix}. \tag{25}$$

Remark. Notice that $\dot{\boldsymbol{\mathcal{U}}} = \boldsymbol{\mathcal{F}}_0(\boldsymbol{\mathcal{U}})$ corresponds to the Kepler problem after the rotation, Levi-Civita and rescaling changes, so system (24) is written as the Kepler problem plus the perturbation $K\boldsymbol{\mathcal{F}}_1(\boldsymbol{\mathcal{U}})$, with K not necessarily small, where $\boldsymbol{\mathcal{F}}_1(\boldsymbol{\mathcal{U}})$ only depends on the position variables, $\boldsymbol{\mathcal{F}}_1(\boldsymbol{\mathcal{U}}) = \boldsymbol{\mathcal{F}}_1(\mathcal{U}, \mathcal{V})$.

At this point, our next goal is to find the solution as $\boldsymbol{\mathcal{U}} = \boldsymbol{\mathcal{U}}_0 + \boldsymbol{\mathcal{U}}_1$ where $\boldsymbol{\mathcal{U}}_0$ is the solution of the 2-body problem

$$\dot{\boldsymbol{\mathcal{U}}}_0 = \boldsymbol{\mathcal{F}}_0(\boldsymbol{\mathcal{U}}_0), \tag{26}$$

and $\boldsymbol{\mathcal{U}}_1$ is the solution of

$$\dot{\boldsymbol{\mathcal{U}}}_1 = K\boldsymbol{\mathcal{F}}_1(\boldsymbol{\mathcal{U}}_0 + \boldsymbol{\mathcal{U}}_1) + \boldsymbol{\mathcal{F}}_0(\boldsymbol{\mathcal{U}}_0 + \boldsymbol{\mathcal{U}}_1) - \boldsymbol{\mathcal{F}}_0(\boldsymbol{\mathcal{U}}_0). \tag{27}$$

Note that we are interested only in the ejection orbits, denoted by $\boldsymbol{\mathcal{U}}^e = \boldsymbol{\mathcal{U}}_0^e + \boldsymbol{\mathcal{U}}_1^e$. Due to the change of variables and time given in (22), the initial conditions of these orbits (17) now become

$$\boldsymbol{\mathcal{U}}_0^e(0) = (0, 0, n\cos\theta_0, n\sin\theta_0) \quad \text{and} \quad \boldsymbol{\mathcal{U}}_1^e(0) = \mathbf{0}. \tag{28}$$

For simplicity we will write $\boldsymbol{\mathcal{U}}_0^e(\mathcal{T}) = \boldsymbol{\mathcal{U}}_0^e(n, \theta_0, \mathcal{T})$ and $\boldsymbol{\mathcal{U}}_1^e(\mathcal{T}) = \boldsymbol{\mathcal{U}}_1^e(n, \theta_0, \mathcal{T})$.

In a similar way as we defined M_{LC}, we can define the angular momentum $\mathcal{M}$ in the new coordinates as

$$\mathcal{M} = \mathcal{U}\dot{\mathcal{V}} - \mathcal{V}\dot{\mathcal{U}}. \tag{29}$$

Note that $\mathcal{M}$ is directly related with M_{LC} by

$$M_{LC} = \frac{4}{\sqrt{L}n^{4/3}}\mathcal{M}. \tag{30}$$

Definition 4. For any fixed value n, let $\boldsymbol{\mathcal{U}}$ be a solution of system (23) with initial conditions $(0, 0, n\cos\theta_0, n\sin\theta_0)$. We define $\mathcal{M}(n, \theta_0)$ as the value of the angular momentum (29) of the ejection orbit with ejection angle θ_0 at the nth minimum in the distance to the nucleus.

So the strategy of the proof is, using Proposition 1 and Lemma 1, to find the values of θ_0 such that $\mathcal{M}(n, \theta_0) = 0$. We show in Fig. 4, left, the curve $(\theta_0, M_{LC}(n, \theta_0))$, for $n = 1, 2$ for a specific value of C. Notice that we only consider $\theta_0 \in [0, \pi)$ due to doubling configuration plane in Levi-Civita (or ad hoc $(\mathcal{U}, \mathcal{V})$ variables). We see that the curve crosses twice the $M_{LC} = 0$ axis, so there are two specific values of θ_0 such that correspond to n-EC orbits, plotted on the right.

In order to compute the angular momentum $\mathcal{M}(n, \theta_0)$, we follow the next steps. We give here a summary of each of them, we refer the reader to Appendix B for the details of the proofs.

(i) First, we compute the solution $\mathcal{U}_0^e(\mathcal{T})$ of the unperturbed system (26). Notice that, although it is an integrable system, it is not straight to find explicit solutions. To find $\mathcal{U}_0^e$, first we solve the 2-body problem in sidereal (non rotating) Levi-Civita coordinates (in such a case we know the explicit expression of the solution), second, we apply the rotation transformation to move from the sidereal coordinates to the synodical (rotating) ones plus the change (22). Finally, considering the initial conditions (28) for the specific case of the ejection orbits we obtain

$$\begin{cases} \mathcal{U}_0^e(\mathcal{T}) = \left[\cos\theta_0 \cos(-t/2) - \sin\theta_0 \sin(-t/2)\right] \sin(n\mathcal{T}), \\ \mathcal{V}_0^e(\mathcal{T}) = \left[\cos\theta_0 \sin(-t/2) + \sin\theta_0 \cos(-t/2)\right] \sin(n\mathcal{T}), \end{cases} \tag{31}$$

with

$$t = 2\left[\mathcal{T} - \frac{\cos(n\mathcal{T})\sin(n\mathcal{T})}{n}\right]\varepsilon^3. \tag{32}$$

Recall that t is the time in the sidereal system, so (32) relates the sidereal time t with the rescaled time $\mathcal{T}$. The details of this step are done in Appendix B.1.

Remark. Notice that from (31) it is very easy to obtain that the nth minimum distance will be reached when

$$\mathcal{T} = \mathcal{T}_0^* = \pi. \tag{33}$$

(ii) Second, we compute the solution $\mathcal{U}_1^e(\mathcal{T})$ of the perturbed problem (27) with initial conditions as in (28). To do so we rewrite system (27) as

$$\dot{\mathcal{U}}_1 = D\mathcal{F}_0(\mathcal{U}_0)\mathcal{U}_1 + \mathcal{G}(\mathcal{U}_1), \tag{34}$$

where $\mathcal{U}_0 = \mathcal{U}_0^e$ is the ejection solution (31) of the two body problem and

$$\mathcal{G}(\mathcal{U}_1) = K\mathcal{F}_1(\mathcal{U}_0^e + \mathcal{U}_1) + \mathcal{F}_0(\mathcal{U}_0^e + \mathcal{U}_1) - \mathcal{F}_0(\mathcal{U}_0^e) - D\mathcal{F}_0(\mathcal{U}_0^e)\mathcal{U}_1. \tag{35}$$

Note that the ejection solution $\mathcal{U}_1^e$ has zero initial condition and therefore, it is the solution of the implicit equation

$$\mathcal{U}_1^e = \mathcal{H}\{\mathcal{U}_1^e\}, \tag{36}$$

where

$$\mathcal{H}\{\mathcal{U}\}(\mathcal{T}) = X(\mathcal{T}) \int_0^{\mathcal{T}} X^{-1}(\tau)\mathcal{G}(\mathcal{U}(\tau))\, d\tau, \tag{37}$$

and $X(\mathcal{T})$ is the fundamental matrix of the linear system:

$$\dot{\mathcal{U}}_1 = D\mathcal{F}_0(\mathcal{U}_0^e)\mathcal{U}_1. \tag{38}$$

The technical strategy at this point is to apply a Fixed Point Theorem to Eq. (36) to prove the existence of the solution $\mathcal{U}_1^e$. The details of the proof are done in Appendix B.2.

(iii) Next, we compute the time $\mathcal{T}^*$ to reach the nth minimum distance to the origin. In Lemma 9 we prove that

$$\mathcal{T}^* = \mathcal{T}_0^* + \mathcal{T}_1^* = \pi - \frac{3K\pi\cos(2\theta_0)}{n^{4/3}}\varepsilon^4 + \frac{K}{n^{4/3}}\mathcal{O}(\varepsilon^7), \tag{39}$$

where the $\mathcal{O}$ notation denotes uniformity in $1/n^{1/3}$.

(iv) Finally, we compute the angular momentum of the ejection solution $\mathcal{U}^e = \mathcal{U}_0^e + \mathcal{U}_1^e$ at time $\mathcal{T} = \mathcal{T}^*$. The expression obtained is

$$\mathcal{M}(n, \theta_0) = \frac{3K\pi n^{2/3}\sin(2\theta_0)}{2}\varepsilon^4 + Kn^{2/3}\mathcal{O}(\varepsilon^7). \tag{40}$$

The details of the proof are in Lemma 10 in Appendix B.2.

In this way, applying the Implicit Function Theorem, we have that for $\varepsilon \geq 0$ small enough $\mathcal{M}(n, \theta_0)$ has two and only two roots in $[0, \pi)$ given by

$$\theta_0 = \frac{\pi m}{2} + \mathcal{O}(\varepsilon^3), \qquad m = 0, 1, \tag{41}$$

regardless of the values of the parameter $K > 0$ and n. It is clear from (40) that the roots θ_0 are simple, and so we have proved that there exist exactly two n-EC orbits. On the other hand, the symmetry of these two n-EC orbits comes from the symmetry (13a) in the $(\mathcal{U}, \mathcal{V})$ variables.

This concludes the proof of Theorem 1.

Appendix B. Proof of the auxiliary lemmas

So far, we have provided a sketch of the proof of Theorem 1. In this Section, we give the results and the detailed proofs needed to prove the theorem. Recall that the problem, after several changes of coordinates, is given by the system of equations (23).

The section is organized as follows: first, we detail the computation of the solution of the Kepler problem given by Eqs. (26), second we prove the existence of solution for the perturbed problem written as a fixed point problem (36), and then we compute the time to reach the nth minimum distance to the origin.

B.1. Solution of the unperturbed system

We consider Eq. (26):

$$\dot{\mathcal{U}}_0 = \mathcal{F}_0(\mathcal{U}_0),$$

where $\mathcal{F}_0$ is given in (25).

Lemma 2. *The ejection orbits $\mathcal{U}_0^e$, solution of system (26) with initial conditions*

$$\mathcal{U}_0^e(0) = (0, 0, n\cos\theta_0, n\sin\theta_0), \tag{42}$$

are given by

$$\begin{cases} \mathcal{U}_0^e(\mathcal{T}) = \left[\cos\theta_0\cos(-t/2) - \sin\theta_0\sin(-t/2)\right]\sin(n\mathcal{T}), \\ \mathcal{V}_0^e(\mathcal{T}) = \left[\cos\theta_0\sin(-t/2) + \sin\theta_0\cos(-t/2)\right]\sin(n\mathcal{T}), \end{cases} \tag{43}$$

where

$$t = 2\left[\mathcal{T} - \frac{\cos(n\mathcal{T})\sin(n\mathcal{T})}{n}\right]\varepsilon^3. \tag{44}$$

Proof. We must solve the system

$$\begin{cases} \ddot{\mathcal{U}}_0 = -n^2\mathcal{U}_0 + 8(\mathcal{U}_0^2 + \mathcal{V}_0^2)\dot{\mathcal{V}}_0\varepsilon^3 + 12(\mathcal{U}_0^2 + \mathcal{V}_0^2)^2\mathcal{U}_0\varepsilon^6, \\ \ddot{\mathcal{V}}_0 = -n^2\mathcal{V}_0 - 8(\mathcal{U}_0^2 + \mathcal{V}_0^2)\dot{\mathcal{U}}_0\varepsilon^3 + 12(\mathcal{U}_0^2 + \mathcal{V}_0^2)^2\mathcal{V}_0\varepsilon^6, \end{cases} \tag{45}$$

which is the Kepler problem in rotating coordinates, plus a regularization and a rescaling of the variables and time.

First, we consider the Kepler problem in sidereal (non rotating), non-dimensional units, and we introduce Levi-Civita coordinates plus the change of variables (22), $(\bar{\mathcal{U}}_0, \bar{\mathcal{V}}_0)$:

$$\begin{cases} \ddot{\bar{\mathcal{U}}}_0 = -\left[n^2 - 4(\bar{\mathcal{U}}_0\dot{\bar{\mathcal{V}}}_0 - \bar{\mathcal{V}}_0\dot{\bar{\mathcal{U}}}_0)\varepsilon^3\right]\bar{\mathcal{U}}_0, \\ \ddot{\bar{\mathcal{V}}}_0 = -\left[n^2 - 4(\bar{\mathcal{U}}_0\dot{\bar{\mathcal{V}}}_0 - \bar{\mathcal{V}}_0\dot{\bar{\mathcal{U}}}_0)\varepsilon^3\right]\bar{\mathcal{V}}_0, \end{cases} \tag{46}$$

where $\dot{} = \frac{d}{d\mathcal{T}}$ and

$$\frac{dt}{d\mathcal{T}} = 4(\bar{\mathcal{U}}_0^2 + \bar{\mathcal{V}}_0^2)\varepsilon^3. \tag{47}$$

Note that system (46) can be directly obtained from system (45) through the relation

$$\begin{cases} \mathcal{U}_0(\mathcal{T}) = \bar{\mathcal{U}}_0(\mathcal{T})\cos(-t/2) - \bar{\mathcal{V}}_0(\mathcal{T})\sin(-t/2), \\ \mathcal{V}_0(\mathcal{T}) = \bar{\mathcal{U}}_0(\mathcal{T})\sin(-t/2) + \bar{\mathcal{V}}_0(\mathcal{T})\cos(-t/2), \\ \dot{\mathcal{U}}_0(\mathcal{T}) = \left[\dot{\bar{\mathcal{U}}}_0 + 2(\bar{\mathcal{U}}_0^2 + \bar{\mathcal{V}}_0^2)\bar{\mathcal{V}}_0\varepsilon^3\right]\cos(-t/2) - \left[\dot{\bar{\mathcal{V}}}_0 - 2(\bar{\mathcal{U}}_0^2 + \bar{\mathcal{V}}_0^2)\bar{\mathcal{U}}_0\varepsilon^3\right]\sin(-t/2), \\ \dot{\mathcal{U}}_0(\mathcal{T}) = \left[\dot{\bar{\mathcal{U}}}_0 + 2(\bar{\mathcal{U}}_0^2 + \bar{\mathcal{V}}_0^2)\bar{\mathcal{V}}_0\varepsilon^3\right]\sin(-t/2) + \left[\dot{\bar{\mathcal{V}}}_0 - 2(\bar{\mathcal{U}}_0^2 + \bar{\mathcal{V}}_0^2)\bar{\mathcal{U}}_0\varepsilon^3\right]\cos(-t/2). \end{cases} \tag{48}$$

Since the rotation required to move from the sidereal coordinate system to the synodic system (or vice versa) is half that in non-regularized systems, due to the duplication of the configuration space that occurs with the Levi-Civita regularization.

Then the solution of (46) with initial conditions $(\bar{\mathcal{U}}_{0,0}, \bar{\mathcal{V}}_{0,0}, \dot{\bar{\mathcal{U}}}_{0,0}, \dot{\bar{\mathcal{V}}}_{0,0})$ at $\mathcal{T} = 0$ is

$$\begin{cases} \bar{\mathcal{U}}_0(\mathcal{T}) = \bar{\mathcal{U}}_{0,0}\cos(\omega\mathcal{T}) + \dfrac{\dot{\bar{\mathcal{U}}}_{0,0}}{\omega}\sin(\omega\mathcal{T}), \\ \bar{\mathcal{V}}_0(\mathcal{T}) = \bar{\mathcal{V}}_{0,0}\cos(\omega\mathcal{T}) + \dfrac{\dot{\bar{\mathcal{V}}}_{0,0}}{\omega}\sin(\omega\mathcal{T}), \end{cases} \tag{49}$$

where $\omega = \sqrt{n^2 - 4(\bar{\mathcal{U}}_{0,0}\dot{\bar{\mathcal{V}}}_{0,0} - \bar{\mathcal{V}}_{0,0}\dot{\bar{\mathcal{U}}}_{0,0})\varepsilon^3}$. It is also well known that the angular momentum is constant

$$\left[\bar{\mathcal{U}}_0\dot{\bar{\mathcal{V}}}_0 - \bar{\mathcal{V}}_0\dot{\bar{\mathcal{U}}}_0\right](\mathcal{T}) = \bar{\mathcal{U}}_{0,0}\dot{\bar{\mathcal{V}}}_{0,0} - \bar{\mathcal{V}}_{0,0}\dot{\bar{\mathcal{U}}}_{0,0}. \tag{50}$$

Then, using (49) and (47) the value $t(\mathcal{T})$ is given by

$$\begin{aligned} t(\mathcal{T}) = 2\Bigg[&\left(\bar{\mathcal{U}}_{0,0}^2 + \bar{\mathcal{V}}_{0,0}^2\right)\left(\mathcal{T} + \frac{\cos(\omega\mathcal{T})\sin(\omega\mathcal{T})}{\omega}\right) + \frac{2\left(\bar{\mathcal{U}}_{0,0}\dot{\bar{\mathcal{U}}}_{0,0} + \bar{\mathcal{V}}_{0,0}\dot{\bar{\mathcal{V}}}_{0,0}\right)}{\omega^2}\sin^2(\omega\mathcal{T}) \\ &+ \frac{\dot{\bar{\mathcal{U}}}_{0,0}^2 + \dot{\bar{\mathcal{V}}}_{0,0}^2}{\omega^2}\left(\mathcal{T} - \frac{\cos(\omega\mathcal{T})\sin(\omega\mathcal{T})}{\omega}\right)\Bigg]\varepsilon^3. \end{aligned} \tag{51}$$

The relation between the sidereal (non rotating) initial conditions and the synodical (rotating) ones can be obtained from (48) putting $\mathcal{T}=0$

$$\begin{cases} \mathcal{U}_{0,0}=\bar{\mathcal{U}}_{0,0}, \\ \mathcal{V}_{0,0}=\bar{\mathcal{V}}_{0,0}, \\ \dot{\mathcal{U}}_{0,0}=\dot{\bar{\mathcal{U}}}_{0,0}+2(\bar{\mathcal{U}}_{0,0}^2+\bar{\mathcal{V}}_{0,0}^2)\bar{\mathcal{V}}_{0,0}\varepsilon^3, \\ \dot{\mathcal{V}}_{0,0}=\dot{\bar{\mathcal{V}}}_{0,0}-2(\bar{\mathcal{U}}_{0,0}^2+\bar{\mathcal{V}}_{0,0}^2)\bar{\mathcal{U}}_{0,0}\varepsilon^3, \end{cases} \qquad \begin{cases} \bar{\mathcal{U}}_{0,0}=\mathcal{U}_{0,0}, \\ \bar{\mathcal{V}}_{0,0}=\mathcal{V}_{0,0}, \\ \dot{\bar{\mathcal{U}}}_{0,0}=\dot{\mathcal{U}}_{0,0}-2(\mathcal{U}_{0,0}^2+\mathcal{V}_{0,0}^2)\mathcal{V}_{0,0}\varepsilon^3, \\ \dot{\bar{\mathcal{V}}}_{0,0}=\dot{\mathcal{V}}_{0,0}+2(\mathcal{U}_{0,0}^2+\mathcal{V}_{0,0}^2)\mathcal{U}_{0,0}\varepsilon^3. \end{cases} \tag{52}$$

We are interested in the particular case of ejection orbits, which have as their initial condition

$$\bar{\boldsymbol{\mathcal{U}}}_{0,0}^e=\boldsymbol{\mathcal{U}}_{0,0}^e=(0,0,n\cos\theta_0,n\sin\theta_0). \tag{53}$$

So the ejection orbits in rotating coordinates, denoted by $\mathcal{U}_0^e(\theta_0,\mathcal{T}),\mathcal{V}_0^e(\theta_0,\mathcal{T})$ are given by:

$$\begin{cases} \mathcal{U}_0^e(\mathcal{T})=\left[\cos\theta_0\cos(-t/2)-\sin\theta_0\sin(-t/2)\right]\sin(n\mathcal{T}), \\ \mathcal{V}_0^e(\mathcal{T})=\left[\cos\theta_0\sin(-t/2)+\sin\theta_0\cos(-t/2)\right]\sin(n\mathcal{T}), \end{cases} \tag{54}$$

with

$$t=2\left[\mathcal{T}-\frac{\cos(n\mathcal{T})\sin(n\mathcal{T})}{n}\right]\varepsilon^3.$$

This finishes the proof of Lemma 2 □

From the above result, we can find an explicit expression for the fundamental matrix of system (38).

Lemma 3. *The fundamental matrix X for system (38)*

$$\dot{\boldsymbol{\mathcal{U}}}_1=D\boldsymbol{\mathcal{F}}_0(\boldsymbol{\mathcal{U}}_0^e)\boldsymbol{\mathcal{U}}_1$$

where $\boldsymbol{\mathcal{U}}_0^e$ is the solution of (26) with initial conditions $(0,0,n\cos\theta_0,n\sin\theta_0)$ can be expressed as

$$X(\mathcal{T})=\begin{pmatrix} \cos(n\mathcal{T})+\mathcal{O}(\varepsilon^3) & \mathcal{O}(\varepsilon^3) & \dfrac{\sin(n\mathcal{T})+\mathcal{O}(\varepsilon^3)}{n} & \dfrac{1}{n}\mathcal{O}(\varepsilon^3) \\ \mathcal{O}(\varepsilon^3) & \cos(n\mathcal{T})+\mathcal{O}(\varepsilon^3) & \dfrac{1}{n}\mathcal{O}(\varepsilon^3) & \dfrac{\sin(n\mathcal{T})+\mathcal{O}(\varepsilon^3)}{n} \\ -n\sin(n\mathcal{T})+n\mathcal{O}(\varepsilon^3) & n\mathcal{O}(\varepsilon^3) & \cos(n\mathcal{T})+\mathcal{O}(\varepsilon^3) & \mathcal{O}(\varepsilon^3) \\ n\mathcal{O}(\varepsilon^3) & -n\sin(n\mathcal{T})+n\mathcal{O}(\varepsilon^3) & \mathcal{O}(\varepsilon^3) & \cos(n\mathcal{T})+\mathcal{O}(\varepsilon^3) \end{pmatrix}.$$

Proof. Consider the general solution $\boldsymbol{\mathcal{U}}_0$ of system (26) given by (48), we can express the fundamental matrix of the system

$$\dot{\boldsymbol{\mathcal{U}}}_1=D\boldsymbol{\mathcal{F}}_0(\boldsymbol{\mathcal{U}}_0)\boldsymbol{\mathcal{U}}_1,$$

as $X=BA$, where

$$B=\begin{pmatrix} \cos(-t/2) & -\sin(-t/2) & 0 & 0 \\ \sin(-t/2) & \cos(-t/2) & 0 & 0 \\ 0 & 0 & \cos(-t/2) & -\sin(-t/2) \\ 0 & 0 & \sin(-t/2) & \cos(-t/2) \end{pmatrix}, \tag{55}$$

and A is the matrix with rows

$$\begin{aligned} \boldsymbol{A}_1(\mathcal{T})&=\left[\frac{\partial\bar{\mathcal{U}}_0}{\partial\boldsymbol{\mathcal{U}}_0(0)}+\frac{\bar{\mathcal{V}}_0}{2}\frac{\partial t}{\partial\boldsymbol{\mathcal{U}}_0(0)}\right](\mathcal{T}), \\ \boldsymbol{A}_2(\mathcal{T})&=\left[\frac{\partial\bar{\mathcal{V}}_0}{\partial\boldsymbol{\mathcal{U}}_0(0)}-\frac{\bar{\mathcal{U}}_0}{2}\frac{dt}{\partial\boldsymbol{\mathcal{U}}_0(0)}\right](\mathcal{T}), \\ \boldsymbol{A}_3(\mathcal{T})&=\left[\frac{\partial\dot{\bar{\mathcal{U}}}_0}{\partial\boldsymbol{\mathcal{U}}_0(0)}+2\left(\bar{\mathcal{U}}_0^2+3\bar{\mathcal{V}}_0^2\right)\varepsilon^3\frac{\partial\bar{\mathcal{V}}_0}{\partial\boldsymbol{\mathcal{U}}_0(0)}+4\bar{\mathcal{U}}_0\bar{\mathcal{V}}_0\varepsilon^3\frac{\partial\bar{\mathcal{U}}_0}{\partial\boldsymbol{\mathcal{U}}_0(0)}+\frac{\dot{\bar{\mathcal{V}}}_0-2(\bar{\mathcal{U}}_0^2+\bar{\mathcal{V}}_0^2)\bar{\mathcal{U}}_0\varepsilon^3}{2}\frac{\partial t}{\partial\boldsymbol{\mathcal{U}}_0(0)}\right](\mathcal{T}), \\ \boldsymbol{A}_4(\mathcal{T})&=\left[\frac{\partial\dot{\bar{\mathcal{V}}}_0}{\partial\boldsymbol{\mathcal{U}}_0(0)}-2\left(3\bar{\mathcal{U}}_0^2+\bar{\mathcal{V}}_0^2\right)\varepsilon^3\frac{\partial\bar{\mathcal{U}}_0}{\partial\boldsymbol{\mathcal{U}}_0(0)}-4\bar{\mathcal{U}}_0\bar{\mathcal{V}}_0\varepsilon^3\frac{\partial\bar{\mathcal{V}}_0}{\partial\boldsymbol{\mathcal{U}}_0(0)}-\frac{\dot{\bar{\mathcal{U}}}_0+2(\bar{\mathcal{U}}_0^2+\bar{\mathcal{V}}_0^2)\bar{\mathcal{V}}_0\varepsilon^3}{2}\frac{\partial t}{\partial\boldsymbol{\mathcal{U}}_0(0)}\right](\mathcal{T}), \end{aligned} \tag{56}$$

where $\bar{\boldsymbol{\mathcal{U}}}_0$ is given by (49) and t by (51).

We consider an ejection orbit $\boldsymbol{\mathcal{U}}=\boldsymbol{\mathcal{U}}_0^e$, that has initial conditions $(0,0,n\cos\theta_0,n\sin\theta_0)$. Then, the fundamental matrix X can be expressed as $X=B^eA^e$ with

$$A^e=\begin{pmatrix} \cos(n\mathcal{T})+\mathcal{O}(\varepsilon^3) & \mathcal{O}(\varepsilon^3) & \dfrac{\sin(n\mathcal{T})+\mathcal{O}(\varepsilon^3)}{n} & \dfrac{1}{n}\mathcal{O}(\varepsilon^3) \\ \mathcal{O}(\varepsilon^3) & \cos(n\mathcal{T})+\mathcal{O}(\varepsilon^3) & \dfrac{1}{n}\mathcal{O}(\varepsilon^3) & \dfrac{\sin(n\mathcal{T})+\mathcal{O}(\varepsilon^3)}{n} \\ -n\sin(n\mathcal{T})+n\mathcal{O}(\varepsilon^3) & n\mathcal{O}(\varepsilon^3) & \cos(n\mathcal{T})+\mathcal{O}(\varepsilon^3) & \mathcal{O}(\varepsilon^3) \\ n\mathcal{O}(\varepsilon^3) & -n\sin(n\mathcal{T})+n\mathcal{O}(\varepsilon^3) & \mathcal{O}(\varepsilon^3) & \cos(n\mathcal{T})+\mathcal{O}(\varepsilon^3) \end{pmatrix},$$

and

$$B^e = Id + \begin{pmatrix} \mathcal{O}(\varepsilon^6) & \mathcal{O}(\varepsilon^3) & 0 & 0 \\ \mathcal{O}(\varepsilon^3) & \mathcal{O}(\varepsilon^6) & 0 & 0 \\ 0 & 0 & \mathcal{O}(\varepsilon^6) & \mathcal{O}(\varepsilon^3) \\ 0 & 0 & \mathcal{O}(\varepsilon^3) & \mathcal{O}(\varepsilon^6) \end{pmatrix}.$$

Note that the explicit elements of A^e are provided in Appendix C, but, for our purpose, it is enough to consider this expression.

This concludes the proof. □

B.2. The perturbed problem

The objective is to prove the existence of a solution $\boldsymbol{\mathcal{U}}_1^e$ for Eq. (36)

$$\boldsymbol{\mathcal{U}}_1^e = \boldsymbol{\mathcal{H}}\{\boldsymbol{\mathcal{U}}_1^e\},$$

where $\boldsymbol{\mathcal{H}}$ is defined in (37). The strategy is to apply a Fixed Point Theorem.

B.2.1. Preliminaries

We consider the space $\chi = \{\boldsymbol{f} : [0,T] \longrightarrow \mathbb{R}^4, \boldsymbol{f} \text{ continuous}\}$, for a given T. For any function $\boldsymbol{f} = (f_1, \dots, f_4) \in \chi$ we consider the norm:

$$\|\boldsymbol{f}\| = \sup_{\mathcal{T}\in[0,T]} \left(n^{1/3}|f_1(\mathcal{T})| + n^{1/3}|f_2(\mathcal{T})| + \frac{|f_3(\mathcal{T})|}{n^{2/3}} + \frac{|f_4(\mathcal{T})|}{n^{2/3}} \right). \tag{57}$$

Then, χ with this norm is a Banach space. Recall that the time to reach the minimum distance to the origin for the unperturbed problem is $T_0^* = \pi$, (33). Therefore, any fixed value of $T > \pi$ might be taken, for example, we will fix $T = 2\pi$.

Given an $R > 0$, we define the ball $B_R(\mathbf{0}) \subset \chi$ as the set of functions $\boldsymbol{\mathcal{U}} \in \chi$ such that $\|\boldsymbol{\mathcal{U}}\| \le R$.

Given a matrix $A = (a_{ij})_{i,j=1,\dots,4}$, or a vector $\boldsymbol{v} = (v_1, \dots, v_4)$ we denote

$$|A| = (|a_{ij}|)_{i,j=1,\dots,4}, \qquad |\boldsymbol{v}| = (|v_1|, \dots, |v_4|).$$

Given two vectors $\boldsymbol{v} = (v_1, \dots, v_4)$, $\boldsymbol{w} = (w_1, \dots, w_4)$, we will say that

$$\boldsymbol{v} \le \boldsymbol{w} \quad \text{if} \quad v_i \le w_i \quad \forall i = 1, \dots, 4.$$

Similarly with matrices $A \le B$. With this notation we have:

$$|A\boldsymbol{v}| \le |A||\boldsymbol{v}|.$$

Along the following proofs we will use M_i, $i = 1, 2, \dots$, to denote any constant which appears in the bounds which is independent of ε and $n \in \mathbb{N}$.

B.2.2. Fixed point problem

In order to guarantee the existence of the solution $\boldsymbol{\mathcal{U}}_1^e$ of Eq. (36) in the space χ, we must show that the required hypotheses for the Fixed Point Theorem are satisfied.

Proposition 2. *Consider $\boldsymbol{\mathcal{H}}$ defined in (37). There exists a suitable value of R such that the operator $\boldsymbol{\mathcal{H}}$ applies $B_R(\mathbf{0})$ to itself, that is,*

$$\boldsymbol{\mathcal{H}} : B_R(\mathbf{0}) \to B_R(\mathbf{0})$$

and it is a contraction. Therefore there exists a unique $\boldsymbol{\mathcal{U}}_1^e \in B_R(\mathbf{0})$ which is solution of Eq. (36) in χ.

The proof of the proposition is a consequence of the following lemmas.

Lemma 4. *There exist $\varepsilon_0 > 0$ and a constant $M_1 > 0$ such that, for $\varepsilon \in (0, \varepsilon_0)$ and $n \in \mathbb{N}$,*

$$\|\boldsymbol{\mathcal{H}}\{\mathbf{0}\}\| \le M_1 K \varepsilon^4$$

where $\|\cdot\|$ is the norm defined in (57).

Proof. From (35) and (37) we have

$$\boldsymbol{\mathcal{H}}\{\mathbf{0}\}(\mathcal{T}) = X(\mathcal{T}) \int_0^{\mathcal{T}} X^{-1}(\tau)\boldsymbol{\mathcal{G}}(\mathbf{0})\, d\tau = KX(\mathcal{T}) \int_0^{\mathcal{T}} X^{-1}(\tau)\boldsymbol{\mathcal{F}}_1(\boldsymbol{\mathcal{U}}_0^e(\tau))\, d\tau, \tag{58}$$

so we need to bound the components of $\boldsymbol{\mathcal{F}}_1(\boldsymbol{\mathcal{U}}_0^e)$ given by (25). From (31) we have that,

$$(\mathcal{U}_0^e(\theta_0, \tau))^2 + (\mathcal{V}_0^e(\theta_0, \tau))^2 = \sin^2(n\tau) \le 1.$$

so for ε small enough:

$$|\boldsymbol{\mathcal{F}}_1(\mathcal{U}_0^e, \mathcal{V}_0^e)| = 8n^{2/3} \begin{pmatrix} 0 \\ 0 \\ |\mathcal{U}_0^e|^3\varepsilon^4 \\ |\mathcal{V}_0^e|^3\varepsilon^4 \end{pmatrix} \le 8n^{2/3}\varepsilon^4 \begin{pmatrix} 0 \\ 0 \\ 1 \\ 1 \end{pmatrix}. \tag{59}$$

By Lemma 3 we can bound $|X| \leq \mathcal{R}$ and $|X^{-1}| \leq \mathcal{R}$ where

$$\mathcal{R} = \begin{pmatrix} 1+\mathcal{O}(\varepsilon^3) & \mathcal{O}(\varepsilon^3) & \frac{1+\mathcal{O}(\varepsilon^3)}{n} & \frac{1}{n}\mathcal{O}(\varepsilon^3) \\ \mathcal{O}(\varepsilon^3) & 1+\mathcal{O}(\varepsilon^3) & \frac{1}{n}\mathcal{O}(\varepsilon^3) & \frac{1+\mathcal{O}(\varepsilon^3)}{n} \\ n+n\mathcal{O}(\varepsilon^3) & n\mathcal{O}(\varepsilon^3) & 1+\mathcal{O}(\varepsilon^3) & \mathcal{O}(\varepsilon^3) \\ n\mathcal{O}(\varepsilon^3) & n+n\mathcal{O}(\varepsilon^3) & \mathcal{O}(\varepsilon^3) & 1+\mathcal{O}(\varepsilon^3) \end{pmatrix}. \tag{60}$$

In this way, we have

$$|X^{-1}(\tau)\boldsymbol{\mathcal{F}}_1(\mathcal{U}_0^e(\tau), \mathcal{V}_0^e(\tau))| \leq \mathcal{R}|\boldsymbol{\mathcal{F}}_1(\mathcal{U}_0^e(\tau), \mathcal{V}_0^e(\tau))| \leq M\varepsilon^4 \begin{pmatrix} 1/n^{1/3} \\ 1/n^{1/3} \\ n^{2/3} \\ n^{2/3} \end{pmatrix}, \tag{61}$$

for a constant M independent of n. Therefore, for any $\mathcal{T} \leq T = 2\pi$ we have that

$$|\boldsymbol{\mathcal{H}}\{\mathbf{0}\}| \leq MK\varepsilon^4 \begin{pmatrix} 1/n^{1/3} \\ 1/n^{1/3} \\ n^{2/3} \\ n^{2/3} \end{pmatrix}, \tag{62}$$

for a constant M independent of n. Using the definition of the norm in (57) and renaming $M_1 = M$ we conclude the proof. □

Next step is to bound $\boldsymbol{\mathcal{H}}(\boldsymbol{\mathcal{U}}_\oplus) - \boldsymbol{\mathcal{H}}(\boldsymbol{\mathcal{U}}_\ominus)$ for $\boldsymbol{\mathcal{U}}_\oplus$, $\boldsymbol{\mathcal{U}}_\ominus \in B_R(\mathbf{0})$, for a certain ball. First we need a bound for $\boldsymbol{\mathcal{G}}(\boldsymbol{\mathcal{U}}_\oplus) - \boldsymbol{\mathcal{G}}(\boldsymbol{\mathcal{U}}_\ominus)$ defined in (35). We write

$$\boldsymbol{\mathcal{G}}(\boldsymbol{\mathcal{U}}_1) = \boldsymbol{\mathcal{G}}_0(\boldsymbol{\mathcal{U}}_1) + \boldsymbol{\mathcal{G}}_1(\boldsymbol{\mathcal{U}}_1), \tag{63}$$

with

$$\begin{aligned} \boldsymbol{\mathcal{G}}_0(\boldsymbol{\mathcal{U}}_1) &= \boldsymbol{\mathcal{F}}_0(\boldsymbol{\mathcal{U}}_0^e(\mathcal{T}) + \boldsymbol{\mathcal{U}}_1) - \boldsymbol{\mathcal{F}}_0(\boldsymbol{\mathcal{U}}_0^e(\mathcal{T})) - D\boldsymbol{\mathcal{F}}_0(\boldsymbol{\mathcal{U}}_0^e(\mathcal{T}))\boldsymbol{\mathcal{U}}_1, \\ \boldsymbol{\mathcal{G}}_1(\boldsymbol{\mathcal{U}}_1) &= K\boldsymbol{\mathcal{F}}_1(\mathcal{U}_0^e(\mathcal{T}) + \mathcal{U}_1, \mathcal{V}_0^e(\mathcal{T}) + \mathcal{V}_1). \end{aligned} \tag{64}$$

We obtain bounds for both operators separately in Lemmas 5 and 6.

Lemma 5. *Consider $\boldsymbol{\mathcal{U}}_\oplus, \boldsymbol{\mathcal{U}}_\ominus \in B_R(\mathbf{0})$ with $R = 2M_1K\varepsilon^4$ and $\boldsymbol{\mathcal{G}}_0$ defined in (64). Then for $\varepsilon > 0$ small enough we have that*

$$|\boldsymbol{\mathcal{G}}_0(\boldsymbol{\mathcal{U}}_\oplus) - \boldsymbol{\mathcal{G}}_0(\boldsymbol{\mathcal{U}}_\ominus)| \leq MKn^{1/3}\varepsilon^7 \|\boldsymbol{\mathcal{U}}_\oplus - \boldsymbol{\mathcal{U}}_\ominus\| \begin{pmatrix} 0 \\ 0 \\ 1 \\ 1 \end{pmatrix},$$

for a certain constant M.

Proof. Notice that the first two components of $\boldsymbol{\mathcal{G}}_0(\boldsymbol{\mathcal{U}})$ are null, that is $\boldsymbol{\mathcal{G}}_0(\boldsymbol{\mathcal{U}}) = (0, 0, \mathcal{G}_0^3, \mathcal{G}_0^4)(\boldsymbol{\mathcal{U}})$. We will do the computations for the component $\mathcal{G}_0^3$, the ones for $\mathcal{G}_0^4$ are similar. Applying the Mean Value Theorem we have that

$$\begin{aligned} &\mathcal{G}_0^3(\boldsymbol{\mathcal{U}}_\oplus) - \mathcal{G}_0^3(\boldsymbol{\mathcal{U}}_\ominus) = \mathcal{F}_0^3(\boldsymbol{\mathcal{U}}_0 + \boldsymbol{\mathcal{U}}_\oplus) - \mathcal{F}_0^3(\boldsymbol{\mathcal{U}}_0 + \boldsymbol{\mathcal{U}}_\ominus) - D\mathcal{F}_0^3(\boldsymbol{\mathcal{U}}_0)(\boldsymbol{\mathcal{U}}_\oplus - \boldsymbol{\mathcal{U}}_\ominus) \\ &= \int_0^1 \left[D\mathcal{F}_0^3(\boldsymbol{\mathcal{U}}_0 + s\boldsymbol{\mathcal{U}}_\oplus + (1-s)\boldsymbol{\mathcal{U}}_\ominus)(\boldsymbol{\mathcal{U}}_\oplus - \boldsymbol{\mathcal{U}}_\ominus)\right] ds - D\mathcal{F}_0^3(\boldsymbol{\mathcal{U}}_0)(\boldsymbol{\mathcal{U}}_\oplus - \boldsymbol{\mathcal{U}}_\ominus) \\ &= \left\{\int_0^1 \left[D\mathcal{F}_0^3(\boldsymbol{\mathcal{U}}_0 + s\boldsymbol{\mathcal{U}}_\oplus + (1-s)\boldsymbol{\mathcal{U}}_\ominus) - D\mathcal{F}_0^3(\boldsymbol{\mathcal{U}}_0)\right] ds\right\}(\boldsymbol{\mathcal{U}}_\oplus - \boldsymbol{\mathcal{U}}_\ominus) \\ &= \left\{\int_0^1 \int_0^1 \left(s\boldsymbol{\mathcal{U}}_\oplus + (1-s)\boldsymbol{\mathcal{U}}_\ominus\right)^t D^2\mathcal{F}_0^3\left(\boldsymbol{\mathcal{U}}_0 + z\left[s\boldsymbol{\mathcal{U}}_\oplus + (1-s)\boldsymbol{\mathcal{U}}_\ominus\right]\right) dz\, ds\right\}(\boldsymbol{\mathcal{U}}_\oplus - \boldsymbol{\mathcal{U}}_\ominus). \end{aligned} \tag{65}$$

We have to bound the expression appearing in the previous double integral. Recall that $D^2\mathcal{F}_0^3$ (see (25)) is given by:

$$D^2\mathcal{F}_0^3 = \begin{pmatrix} 16\left[\dot{\mathcal{V}} + 3(5\mathcal{U}^2 + 3\mathcal{V}^2)\mathcal{U}\varepsilon^3\right]\varepsilon^3 & 48(3\mathcal{U}^2 + \mathcal{V}^2)\mathcal{V}\varepsilon^6 & 0 & 16\mathcal{U}\varepsilon^3 \\ 48(3\mathcal{U}^2 + \mathcal{V}^2)\mathcal{V}\varepsilon^6 & 16\left[\dot{\mathcal{V}} + 3(\mathcal{U}^2 + 3\mathcal{V}^2)\mathcal{U}\varepsilon^3\right]\varepsilon^3 & 0 & 16\mathcal{V}\varepsilon^3 \\ 0 & 0 & 0 & 0 \\ 16\mathcal{U}\varepsilon^3 & 16\mathcal{V}\varepsilon^3 & 0 & 0 \end{pmatrix}.$$

Using (31)

$$|\mathcal{U}_0^e| \leq 1, |\mathcal{V}_0^e| \leq 1, |\dot{\mathcal{U}}_0^e| \leq n, |\dot{\mathcal{V}}_0^e| \leq n,$$

so for any $\|\boldsymbol{\mathcal{U}}_\otimes\| \leq 2M_1K\varepsilon^4$ we have that

$$\left|D^2\mathcal{F}_0^3(\boldsymbol{\mathcal{U}}_0^e + \boldsymbol{\mathcal{U}}_\otimes)\right| \leq M\varepsilon^3 \begin{pmatrix} n & \varepsilon^3 & 0 & 1 \\ \varepsilon^3 & n & 0 & 1 \\ 0 & 0 & 0 & 0 \\ 1 & 1 & 0 & 0 \end{pmatrix}. \tag{66}$$

Now, for any $\|\mathcal{U}_\odot\| \le 2M_1K\varepsilon^4$:

$$\begin{aligned}|\mathcal{U}_\odot^t D^2\mathcal{F}_0^3(\mathcal{U}_0^e+\mathcal{U}_\otimes)| &\le |\mathcal{U}_\odot^t|\,|D^2\mathcal{F}_0^3(\mathcal{U}_0^e+\mathcal{U}_\otimes)|\\ &\le 2M_1K\varepsilon^4\left(1/n^{1/3},\,1/n^{1/3},\,n^{2/3},\,n^{2/3}\right)M\varepsilon^3\begin{pmatrix} n & \varepsilon^3 & 0 & 1\\ \varepsilon^3 & n & 0 & 1\\ 0 & 0 & 0 & 0\\ 1 & 1 & 0 & 0\end{pmatrix}\\ &\le 2MM_1K\varepsilon^7\left(n^{2/3},\,n^{2/3},\,0,\,1/n^{1/3}\right).\end{aligned} \tag{67}$$

Taking into account the integral expression in (65) we obtain

$$\begin{aligned}|\mathcal{G}_0^3(\mathcal{U}_\oplus)-\mathcal{G}_0^3(\mathcal{U}_\ominus)| &\le 2MM_1K\varepsilon^4\left(n^{2/3},\,n^{2/3},\,0,\,1/n^{1/3}\right)|\mathcal{U}_\oplus-\mathcal{U}_\ominus|\\ &= 2MM_1K\varepsilon^7\left(n^{2/3}|\mathcal{U}_\oplus-\mathcal{U}_\ominus|+n^{2/3}|\mathcal{V}_\oplus-\mathcal{V}_\ominus|+\frac{|\dot{\mathcal{V}}_\oplus-\dot{\mathcal{V}}_\ominus|}{n^{1/3}}\right)\\ &\le 2MM_1Kn^{1/3}\varepsilon^7\|\mathcal{U}_\oplus-\mathcal{U}_\ominus\|.\end{aligned}$$

We get a similar bound for the fourth component. □

Lemma 6. *Consider $\mathcal{U}_\oplus, \mathcal{U}_\ominus \in B_R(\mathbf{0})$, with $R = 2M_1K\varepsilon^4$ and $\mathcal{G}_1$ defined in (64). Then for $\varepsilon > 0$ small enough we have that*

$$|\mathcal{G}_1(\mathcal{U}_\oplus)-\mathcal{G}_1(\mathcal{U}_\ominus)| \le MKn^{1/3}\varepsilon^4\|\mathcal{U}_\oplus-\mathcal{U}_\ominus\|\begin{pmatrix}0\\0\\1\\1\end{pmatrix},$$

for a certain constant M.

Proof. Using again the Main Value Theorem we obtain:

$$\mathcal{G}_1(\mathcal{U}_\oplus)-\mathcal{G}_1(\mathcal{U}_\ominus) = \int_0^1 D\mathcal{G}_1(s\mathcal{U}_\oplus+(1-s)\mathcal{U}_\ominus)(\mathcal{U}_\oplus-\mathcal{U}_\ominus)\,ds. \tag{68}$$

So we only need to bound $|D\mathcal{G}_1(\mathcal{U}_\odot)|$ where $\mathcal{U}_\odot \in B_R(\mathbf{0})$. Let us recall that

$$D\mathcal{G}_1(\mathcal{U}_\odot) = KD\boldsymbol{\mathcal{F}}_1(\mathcal{U}_0^e+\mathcal{U}_\odot, \mathcal{V}_0^e+\mathcal{V}_\odot),$$

and $\boldsymbol{\mathcal{F}}_1$ is given in (25). Proceeding similarly as before, we differentiate it to obtain:

$$D\boldsymbol{\mathcal{F}}_1(\mathcal{U},\mathcal{V}) = -48n^{2/3}\varepsilon^4\begin{pmatrix}0&0&0&0\\0&0&0&0\\\mathcal{U}&0&0&0\\0&\mathcal{V}&0&0\end{pmatrix}.$$

So, using again (31) we have that: $|\mathcal{U}_0^e| \le 1, |\mathcal{V}_0^e| \le 1$, and for any $\mathcal{U}_\odot \in B_R(\mathbf{0})$,

$$|D\boldsymbol{\mathcal{F}}_1(\mathcal{U}_0^e+\mathcal{U}_\odot, \mathcal{V}_0^e+\mathcal{V}_\odot)| \le Mn^{2/3}\varepsilon^4\begin{pmatrix}0&0&0&0\\0&0&0&0\\1&0&0&0\\0&1&0&0\end{pmatrix},$$

and therefore

$$|D\mathcal{G}_1(\mathcal{U}_\odot)| \le MKn^{2/3}\varepsilon^4\begin{pmatrix}0&0&0&0\\0&0&0&0\\1&0&0&0\\0&1&0&0\end{pmatrix}.$$

Using the integral equation (68) and the fact that the first two rows of the previous matrix are zero we get:

$$|\mathcal{G}_1(\mathcal{U}_\oplus)-\mathcal{G}_1(\mathcal{U}_\ominus)| \le MKn^{2/3}\varepsilon^4\begin{pmatrix}0\\0\\|\mathcal{U}_\oplus-\mathcal{U}_\ominus|\\|\mathcal{V}_\oplus-\mathcal{V}_\ominus|\end{pmatrix} \le MKn^{1/3}\varepsilon^4\|\mathcal{U}_\oplus-\mathcal{U}_\ominus\|\begin{pmatrix}0\\0\\1\\1\end{pmatrix}.$$ □

Now we can prove that $\boldsymbol{\mathcal{H}}$ is Lipschitz.

Lemma 7. *Given $\varepsilon_0 > 0$ and $M_1 > 0$ as in Lemma 4, there exist $\varepsilon_1 \in (0, \varepsilon_0]$ and a constant $M_2 \ge M_1$ such that, for $\varepsilon \in (0, \varepsilon_1)$ and $n \in \mathbb{N}$, given $\mathcal{U}_\oplus$, $\mathcal{U}_\ominus \in B_R(\mathbf{0})$ with $R = 2M_1K\varepsilon^4$ then*

$$\|\boldsymbol{\mathcal{H}}\{\mathcal{U}_\oplus\}-\boldsymbol{\mathcal{H}}\{\mathcal{U}_\ominus\}\| \le M_2K\varepsilon^4\|\mathcal{U}_\oplus-\mathcal{U}_\ominus\|,$$

where $\|\cdot\|$ is the norm defined in (57).

Proof. Recall that we have written

$$\mathcal{G}(\mathcal{U}_1) = \mathcal{G}_0(\mathcal{U}_1) + \mathcal{G}_1(\mathcal{U}_1),$$

with $\mathcal{G}_0$, $\mathcal{G}_1$ given in (64). From the results of Lemmas 5 and 6 we have:

$$|\mathcal{G}(\mathcal{U}_\oplus) - \mathcal{G}(\mathcal{U}_\ominus)| \le MKn^{1/3}\varepsilon^4 \|\mathcal{U}_\oplus - \mathcal{U}_\ominus\| \begin{pmatrix} 0 \\ 0 \\ 1 \\ 1 \end{pmatrix}.$$

Now, we proceed in the same way as in the proof of Lemma 4 to obtain

$$|\mathcal{H}\{\mathcal{U}_\oplus\} - \mathcal{H}\{\mathcal{U}_\ominus\}| \le MK\varepsilon^4 \|\mathcal{U}_\oplus - \mathcal{U}_\ominus\| \begin{pmatrix} 1/n^{2/3} \\ 1/n^{2/3} \\ n^{1/3} \\ n^{1/3} \end{pmatrix},$$

and therefore:

$$\|\mathcal{H}\{\mathcal{U}_\oplus\} - \mathcal{H}\{\mathcal{U}_\ominus\}\| \le \frac{M_2 K\varepsilon^4}{n^{1/3}} \|\mathcal{U}_\oplus - \mathcal{U}_\ominus\|. \tag{69}$$

This finishes the proof of Lemma 7. □

At this point we select ε_1 such that $M_2 K\varepsilon_1^4 < 1/2$, and we can prove Proposition 2.

Proof. If $\mathcal{U} \in B_R(\mathbf{0})$, then:

$$\|\mathcal{H}\{\mathcal{U}\}\| = \|\mathcal{H}\{\mathbf{0}\} + \mathcal{H}\{\mathcal{U}\} - \mathcal{H}\{\mathbf{0}\}\| \le \|\mathcal{H}\{\mathbf{0}\}\| + \|\mathcal{H}\{\mathcal{U}\} - \mathcal{H}\{\mathbf{0}\}\| \le \frac{R}{2} + \frac{R}{2} = R,$$

and we already know by Lemma 7 that $\mathcal{H}$ is Lipschitz, with Lipschitz constant $M_2 K\varepsilon^4 < 1/2$.

By the Fixed Point Theorem there exists a unique $\mathcal{U}_1^e \in B_R(\mathbf{0})$ which is solution of Eq. (36). □

Observe that once we know the existence and bounds of the function $\mathcal{U}_1^e$, its smoothness is a consequence of being solution of a smooth differential equation.

Therefore, for $\mathcal{U}_1^e$ the solution of the fixed point problem given in Proposition 2, we have that $\|\mathcal{U}_1^e\| \le R = 2M_1 K\varepsilon^4$ and

$$\|\mathcal{U}_1^e - \mathcal{H}\{\mathbf{0}\}\| = \|\mathcal{H}\{\mathcal{U}_1^e\} - \mathcal{H}\{\mathbf{0}\}\| \le M_2 K\varepsilon^4 \|\mathcal{U}_1^e\| \le 2M_1 M_2 K^2 \varepsilon^8.$$

In particular, and using the definition of the norm (57), we can write

$$\mathcal{U}_1^e = \mathcal{H}\{\mathbf{0}\} + K^2 \begin{pmatrix} n^{-1/3} \\ n^{-1/3} \\ n^{2/3} \\ n^{2/3} \end{pmatrix} \mathcal{O}(\varepsilon^8). \tag{70}$$

Lemma 8. *With the same hypotheses of Lemma 7, $\mathcal{H}\{\mathbf{0}\}(\mathcal{T}) = (\mathcal{H}_1, \mathcal{H}_2, \mathcal{H}_3, \mathcal{H}_4)\{\mathbf{0}\}(\mathcal{T})$ where*

$$\begin{aligned} \mathcal{H}_1\{\mathbf{0}\}(\mathcal{T}) &= \mathcal{H}_1^4(\mathcal{T})\varepsilon^4 + \frac{K}{n^{1/3}}\mathcal{O}(\varepsilon^7), \\ \mathcal{H}_2\{\mathbf{0}\}(\mathcal{T}) &= \mathcal{H}_2^4(\mathcal{T})\varepsilon^4 + \frac{K}{n^{1/3}}\mathcal{O}(\varepsilon^7), \\ \mathcal{H}_3\{\mathbf{0}\}(\mathcal{T}) &= \mathcal{H}_3^4(\mathcal{T})\varepsilon^4 + Kn^{2/3}\mathcal{O}(\varepsilon^7), \\ \mathcal{H}_4\{\mathbf{0}\}(\mathcal{T}) &= \mathcal{H}_4^4(\mathcal{T})\varepsilon^4 + Kn^{2/3}\mathcal{O}(\varepsilon^7), \end{aligned} \tag{71}$$

with

$$\mathcal{H}_1^4(\mathcal{T}) = -\frac{K\cos^3\theta_0 \cos(n\mathcal{T})\left[\cos(n\mathcal{T})\sin(n\mathcal{T}) - 3n\mathcal{T}\right]}{n^{4/3}},$$

$$\mathcal{H}_2^4(\mathcal{T}) = \frac{K\sin^3\theta_0 \cos(n\mathcal{T})\left[\cos(n\mathcal{T})\sin(n\mathcal{T}) - 3n\mathcal{T}\right]}{n^{4/3}},$$

$\mathcal{H}_3^4 = \dfrac{d\mathcal{H}_1^4}{d\mathcal{T}}$ *and* $\mathcal{H}_4^4 = \dfrac{d\mathcal{H}_2^4}{d\mathcal{T}}$.

Proof. Recall that, from its definition (37),

$$\mathcal{H}\{\mathbf{0}\}(\mathcal{T}) = X(\mathcal{T}) \int_0^{\mathcal{T}} X^{-1}(\tau)\mathcal{G}(\mathbf{0})\, d\tau = KX(\mathcal{T}) \int_0^{\mathcal{T}} X^{-1}(\tau)\mathcal{F}_1(\mathcal{U}_0^e(\tau))\, d\tau,$$

where $\mathcal{F}_1$ is given in (25). Using (31) we have

$$\mathcal{F}_1(\mathcal{U}_0^e(\tau), \mathcal{V}_0^e(\tau)) = \begin{pmatrix} 0 \\ 0 \\ -8n^{2/3}\cos^3\theta_0 \sin^3(n\tau)\varepsilon^4 + n^{2/3}\mathcal{O}(\varepsilon^7) \\ 8n^{2/3}\sin^3\theta_0 \sin^3(n\tau)\varepsilon^4 + n^{2/3}\mathcal{O}(\varepsilon^7) \end{pmatrix}.$$

Multiplying by X^{-1} (see Lemma 3) we obtain

$$X^{-1}(\tau)\boldsymbol{\mathcal{F}}_1(\mathcal{U}_0^e(\tau),\mathcal{V}_0^e(\tau)) = \begin{pmatrix} 8n^{-1/3}\cos^3\theta_0\sin^4(n\tau) \\ -8n^{-1/3}\sin^3\theta_0\sin^4(n\tau) \\ -8n^{2/3}\cos^3\theta_0\cos(n\tau)\sin^3(n\mathcal{T}) \\ 8n^{2/3}\sin^3\theta_0\cos(n\tau)\sin^3(n\mathcal{T}) \end{pmatrix}\varepsilon^4 + \begin{pmatrix} n^{-1/3} \\ n^{-1/3} \\ n^{2/3} \\ n^{2/3} \end{pmatrix}\mathcal{O}(\varepsilon^7).$$

Finally, integrating until time $\mathcal{T}$ and multiplying by $KX(\mathcal{T})$ we obtain $\boldsymbol{\mathcal{H}}\{\mathbf{0}\}(\mathcal{T})$. □

Combining (70) and Lemma 8, we have that $\boldsymbol{\mathcal{U}}_1^e = \boldsymbol{\mathcal{U}}_1^{4,e}\varepsilon^4 + \mathcal{O}(\varepsilon^7)$, where the terms of order 4 are the same as the terms of order 4 of $\boldsymbol{\mathcal{H}}\{\mathbf{0}\}$. That is, we can write

$$\begin{aligned} \mathcal{U}_1^e(\mathcal{T}) &= \mathcal{U}_1^{4,e}(\mathcal{T})\varepsilon^4 + \frac{K}{n^{1/3}}\mathcal{O}(\varepsilon^7), \\ \mathcal{V}_1^e(\mathcal{T}) &= \mathcal{V}_1^{4,e}(\mathcal{T})\varepsilon^4 + \frac{K}{n^{1/3}}\mathcal{O}(\varepsilon^7), \\ \dot{\mathcal{U}}_1^e(\mathcal{T}) &= \dot{\mathcal{U}}_1^{4,e}(\mathcal{T})\varepsilon^4 + Kn^{2/3}\mathcal{O}(\varepsilon^7), \\ \dot{\mathcal{V}}_1^e(\mathcal{T}) &= \dot{\mathcal{V}}_1^{4,e}(\mathcal{T})\varepsilon^4 + Kn^{2/3}\mathcal{O}(\varepsilon^7), \end{aligned} \tag{72}$$

where $\boldsymbol{\mathcal{U}}_1^{4,e} = (\mathcal{U}_1^e, \mathcal{V}_1^{4,e}, \dot{\mathcal{U}}_1^e, \dot{\mathcal{V}}_1^e) = (\mathcal{H}_1^4, \mathcal{H}_2^4, \mathcal{H}_3^4, \mathcal{H}_4^4)$ given in Lemma 8. In particular, for $\mathcal{T} = \mathcal{T}_0^* = \pi$:

$$\begin{aligned} \mathcal{U}_1^{4,e}(\mathcal{T}_0^*) &= \frac{3K(-1)^n\pi\cos^3\theta_0}{n^{1/3}}, & \mathcal{V}_1^{4,e}(\mathcal{T}_0^*) &= -\frac{3K(-1)^n\pi\sin^3\theta_0}{n^{1/3}}, \\ \dot{\mathcal{U}}_1^{4,e}(\mathcal{T}_0^*) &= \frac{2K(-1)^n\cos^3\theta_0}{n^{1/3}}, & \dot{\mathcal{V}}_1^{4,e}(\mathcal{T}_0^*) &= -\frac{2K(-1)^n\sin^3\theta_0}{n^{1/3}}. \end{aligned} \tag{73}$$

Therefore, the ejection solution $\boldsymbol{\mathcal{U}}^e = \boldsymbol{\mathcal{U}}_0^e + \boldsymbol{\mathcal{U}}_1^e$ of the problem (24) can be written as:

$$\begin{aligned} \mathcal{U}^e(\mathcal{T}) &= \mathcal{U}_0^e(\mathcal{T}) + \mathcal{U}_1^{4,e}(\mathcal{T})\varepsilon^4 + \frac{K}{n^{1/3}}\mathcal{O}(\varepsilon^7), \\ \mathcal{V}^e(\mathcal{T}) &= \mathcal{V}_0^e(\mathcal{T}) + \mathcal{V}_1^{4,e}(\mathcal{T})\varepsilon^4 + \frac{K}{n^{1/3}}\mathcal{O}(\varepsilon^7), \\ \dot{\mathcal{U}}^e(\mathcal{T}) &= \dot{\mathcal{U}}_0^e(\mathcal{T}) + \dot{\mathcal{U}}_1^{4,e}(\mathcal{T})\varepsilon^4 + Kn^{2/3}\mathcal{O}(\varepsilon^7), \\ \dot{\mathcal{V}}^e(\mathcal{T}) &= \dot{\mathcal{V}}_0^e(\mathcal{T}) + \dot{\mathcal{V}}_1^{4,e}(\mathcal{T})\varepsilon^4 + Kn^{2/3}\mathcal{O}(\varepsilon^7). \end{aligned} \tag{74}$$

Once we have the expression of the ejection solution, we can compute the time needed to reach the nth minimum of the distance to the origin.

Lemma 9. *With the same hypotheses of Lemma 7, the time $\mathcal{T}^*$ needed for the ejection solution $\boldsymbol{\mathcal{U}}^e$ to reach the nth minimum in the distance to the origin is given by $\mathcal{T}^* = \mathcal{T}_0^* + \mathcal{T}_1^*$, where $\mathcal{T}_0^* = \pi$ and:*

$$\mathcal{T}_1^* = -\frac{3K\pi\cos(2\theta_0)}{n^{4/3}}\varepsilon^4 + \frac{K}{n^{4/3}}\mathcal{O}(\varepsilon^7). \tag{75}$$

Proof. In order to compute the time $\mathcal{T}^* = \mathcal{T}_0^* + \mathcal{T}_1^*$ where the n minimum in the distance to the origin takes place, we have to solve

$$\begin{aligned} 0 &= \left(\mathcal{U}^e\dot{\mathcal{U}}^e + \mathcal{V}^e\dot{\mathcal{V}}^e\right)(\mathcal{T}^*) \\ &= \left([\mathcal{U}_0^e + \mathcal{U}_1^e][\dot{\mathcal{U}}_0^e + \dot{\mathcal{U}}_1^e] + [\mathcal{V}_0^e + \mathcal{V}_1^e][\dot{\mathcal{V}}_0^e + \dot{\mathcal{V}}_1^e]\right)(\mathcal{T}^*) \\ &= \left(\mathcal{U}_0^e\dot{\mathcal{U}}_0^e + \mathcal{V}_0^e\dot{\mathcal{V}}_0^e\right)(\mathcal{T}^*) + \varepsilon^4\left(\mathcal{U}_0^e\dot{\mathcal{U}}_1^{4,e} + \mathcal{U}_1^{4,e}\dot{\mathcal{U}}_0^e + \mathcal{V}_0^e\dot{\mathcal{V}}_1^{4,e} + \mathcal{V}_1^{4,e}\dot{\mathcal{V}}_0^e\right)(\mathcal{T}^*) + Kn^{2/3}\mathcal{O}(\varepsilon^7) \\ &\quad + \varepsilon^8\left(\mathcal{U}_1^{4,e}\dot{\mathcal{U}}_1^{4,e} + \mathcal{V}_1^{4,e}\dot{\mathcal{V}}_1^{4,e}\right)(\mathcal{T}^*) + K^2n^{1/3}\mathcal{O}(\varepsilon^8) \\ &= \left(\mathcal{U}_0^e\dot{\mathcal{U}}_0^e + \mathcal{V}_0^e\dot{\mathcal{V}}_0^e\right)(\mathcal{T}^*) + \varepsilon^4\left(\mathcal{U}_0^e\dot{\mathcal{U}}_1^{4,e} + \mathcal{U}_1^{4,e}\dot{\mathcal{U}}_0^e + \mathcal{V}_0^e\dot{\mathcal{V}}_1^{4,e} + \mathcal{V}_1^{4,e}\dot{\mathcal{V}}_0^e\right)(\mathcal{T}^*) + Kn^{2/3}\mathcal{O}(\varepsilon^7) \\ &= \left(\mathcal{U}_0^e\dot{\mathcal{U}}_0^e + \mathcal{V}_0^e\dot{\mathcal{V}}_0^e\right)(\mathcal{T}_0^* + \mathcal{T}_1^*) + \varepsilon^4\left(\mathcal{U}_0^e\dot{\mathcal{U}}_1^{4,e} + \mathcal{U}_1^{4,e}\dot{\mathcal{U}}_0^e + \mathcal{V}_0^e\dot{\mathcal{V}}_1^{4,e} + \mathcal{V}_1^{4,e}\dot{\mathcal{V}}_0^e\right)(\mathcal{T}_0^* + \mathcal{T}_1^*) \\ &\quad + Kn^{2/3}\mathcal{O}(\varepsilon^7) \\ &= \left(\mathcal{U}_0^e\dot{\mathcal{U}}_0^e + \mathcal{V}_0^e\dot{\mathcal{V}}_0^e\right)(\mathcal{T}_0^*) + \mathcal{T}_1^*\left(\mathcal{U}_0^e\ddot{\mathcal{U}}_0^e + \dot{\mathcal{U}}_0^{e^2} + \mathcal{V}_0\ddot{\mathcal{V}}_0 + \dot{\mathcal{V}}_0^{e^2}\right)(\mathcal{T}_0^*) \\ &\quad + \varepsilon^4\left(\mathcal{U}_0^e\dot{\mathcal{U}}_1^{4,e} + \mathcal{U}_1^{4,e}\dot{\mathcal{U}}_0^e + \mathcal{V}_0^e\dot{\mathcal{V}}_1^{4,e} + \mathcal{V}_1^{4,e}\dot{\mathcal{V}}_0^e\right)(\mathcal{T}_0^*) + Kn^{2/3}\mathcal{O}(\varepsilon^7) \\ &= \mathcal{T}_1^*n^2 + \varepsilon^4\left(\mathcal{U}_1^{4,e}\dot{\mathcal{U}}_0^e + \mathcal{V}_1^{4,e}\dot{\mathcal{V}}_0^e\right)(\mathcal{T}_0^*) + Kn^{2/3}\mathcal{O}(\varepsilon^7), \end{aligned}$$

and therefore we have

$$\mathcal{T}_1^* = -\frac{\left(\mathcal{U}_1^{4,e}\dot{\mathcal{U}}_0^e + \mathcal{V}_1^{4,e}\dot{\mathcal{V}}_0^e\right)(\mathcal{T}_0^*)}{n^2}\varepsilon^4 + \frac{K}{n^{4/3}}\mathcal{O}(\varepsilon^7) = -\frac{3K\pi\cos(2\theta_0)}{n^{4/3}}\varepsilon^4 + \frac{K}{n^{4/3}}\mathcal{O}(\varepsilon^7). \tag{76}$$

In this way,

$$\mathcal{T}_1^* = \frac{K}{n^{4/3}}\mathcal{O}(\varepsilon^4). \tag{77}$$

This concludes the proof of Lemma 9 □

Finally we can compute the angular momentum at $\mathcal{T}^*$.

Lemma 10. *With the same hypotheses of Lemma 7, the angular momentum of the ejection solution $\mathcal{U}^e$ at time $\mathcal{T}^*$ is given by:*

$$\mathcal{M}(n,\theta_0) = \frac{3K\pi n^{2/3}\sin(2\theta_0)}{2}\varepsilon^4 + Kn^{2/3}\mathcal{O}(\varepsilon^7).$$

Proof. Taking into account the expression of $\mathcal{T}^*$, and those of $\mathcal{U}_0^e(\mathcal{T})$, $\mathcal{U}_1^{4,e}(\mathcal{T})$ and $\mathcal{V}_1^{4,e}(\mathcal{T})$, the angular momentum at $\mathcal{T}^*$ is given by

$$\begin{aligned}
\mathcal{M}(n,\theta_0) &= \left(\mathcal{U}^e\dot{\mathcal{V}}^e - \mathcal{V}^e\dot{\mathcal{U}}^e\right)(\mathcal{T}^*)\\
&= \left(\mathcal{U}_0^e\dot{\mathcal{V}}_0^e - \mathcal{V}_0^e\dot{\mathcal{U}}_0^e\right)(\mathcal{T}^*) + \varepsilon^4\left(\mathcal{U}_0^e\dot{\mathcal{V}}_1^{4,e} + \mathcal{U}_1^{4,e}\dot{\mathcal{V}}_0^e - \mathcal{V}_0^e\dot{\mathcal{U}}_1^{4,e} - \mathcal{V}_1^{4,e}\dot{\mathcal{U}}_0^e\right)(\mathcal{T}^*) + Kn^{2/3}\mathcal{O}(\varepsilon^7)\\
&= \left(\mathcal{U}_0^e\dot{\mathcal{V}}_0^e - \mathcal{V}_0^e\dot{\mathcal{U}}_0^e\right)(\mathcal{T}_0^*) + \mathcal{T}_1^*\left(\mathcal{U}_0^e\ddot{\mathcal{V}}_0^e - \mathcal{V}_0^e\ddot{\mathcal{U}}_0^e\right)(\mathcal{T}_0^*) + K^2n^{1/3}\mathcal{O}(\varepsilon^8)\\
&\quad + \varepsilon^4\left(\mathcal{U}_0^e\dot{\mathcal{V}}_1^{4,e} + \mathcal{U}_1^{4,e}\dot{\mathcal{V}}_0^e - \mathcal{V}_0^e\dot{\mathcal{U}}_1^{4,e} - \mathcal{V}_1^{4,e}\dot{\mathcal{U}}_0^e\right)(\mathcal{T}_0^*) + Kn^{2/3}\mathcal{O}(\varepsilon^7)\\
&= \varepsilon^4\left(\mathcal{U}_1^{4,e}\dot{\mathcal{V}}_0^e - \mathcal{V}_1^{4,e}\dot{\mathcal{U}}_0^e\right)(\mathcal{T}_0^*) + Kn^{2/3}\mathcal{O}(\varepsilon^7)\\
&= \frac{3K\pi n^{2/3}\sin(2\theta_0)}{2}\varepsilon^4 + Kn^{2/3}\mathcal{O}(\varepsilon^7).
\end{aligned}$$

This concludes the proof of Lemma 10 □

Appendix C. Values of the auxiliary matrix of Lemma 3

In what follows we give the values of the terms $(A^e_{i,j})$ of the auxiliary matrix A^e in Lemma 3.

$$\begin{aligned}
A^e_{11} &= \cos(n\mathcal{T}) - \sin(2\theta_0)\left[\mathcal{T}\cos(n\mathcal{T}) - \sin(n\mathcal{T})\frac{1+\sin^2(n\mathcal{T})}{n}\right]\varepsilon^3\\
&\quad + \frac{2\sin^2\theta_0}{n}\left[\mathcal{T}\left(1+2\cos^2(n\mathcal{T})\right) - \frac{3\cos(n\mathcal{T})\sin(n\mathcal{T})}{n}\right]\sin(n\mathcal{T})\varepsilon^6,
\end{aligned}$$

$$\begin{aligned}
A^e_{12} &= 2\left[\cos^2\theta_0\mathcal{T}\cos(n\mathcal{T}) - \frac{\sin(n\mathcal{T})\left(\cos^2\theta_0 - \sin^2\theta_0\sin^2(n\mathcal{T})\right)}{n}\right]\varepsilon^3\\
&\quad - \frac{\sin(2\theta_0)}{n}\left[\mathcal{T}\left(1+2\cos^2(n\mathcal{T})\right) - \frac{3\cos(n\mathcal{T})\sin(n\mathcal{T})}{n}\right]\sin(n\mathcal{T})\varepsilon^6,
\end{aligned}$$

$$A^e_{13} = \frac{\sin(n\mathcal{T})}{n} + \frac{2\sin^2\theta_0}{n}\left[\mathcal{T} - \frac{\cos(n\mathcal{T})\sin(n\mathcal{T})}{n}\right]\sin(n\mathcal{T})\varepsilon^3,$$

$$A^e_{14} = \frac{\sin(2\theta_0)}{n}\left[\mathcal{T} - \frac{\cos(n\mathcal{T})\sin(n\mathcal{T})}{n}\right]\sin(n\mathcal{T})\varepsilon^3,$$

$$\begin{aligned}
A^e_{21} &= -2\left[\sin^2\theta_0\mathcal{T}\cos(n\mathcal{T}) + \frac{\sin(n\mathcal{T})\left(\sin^2\theta_0 - \cos^2\theta_0\sin^2(n\mathcal{T})\right)}{n}\right]\varepsilon^3\\
&\quad - \frac{\sin(2\theta_0)}{n}\left[\mathcal{T}\left(1+2\cos^2(n\mathcal{T})\right) - \frac{3\cos(n\mathcal{T})\sin(n\mathcal{T})}{n}\right]\sin(n\mathcal{T})\varepsilon^6,
\end{aligned}$$

$$\begin{aligned}
A^e_{22} &= \cos(n\mathcal{T}) + \sin(2\theta_0)\left[\mathcal{T}\cos(n\mathcal{T}) - \sin(n\mathcal{T})\frac{1+\sin^2(n\mathcal{T})}{n}\right]\varepsilon^3\\
&\quad + \frac{2\cos^2\theta_0}{n}\left[\mathcal{T}\left(1+2\cos^2(n\mathcal{T})\right) - \frac{3\cos(n\mathcal{T})\sin(n\mathcal{T})}{n}\right]\sin(n\mathcal{T})\varepsilon^6,
\end{aligned}$$

$$A^e_{23} = -\frac{2\cos^2\theta_0}{n}\left[\mathcal{T} - \frac{\cos(n\mathcal{T})\sin(n\mathcal{T})}{n}\right]\sin(n\mathcal{T})\varepsilon^3,$$

$$A^e_{24} = \frac{\sin(n\mathcal{T})}{n} - \frac{\sin(2\theta_0)}{n}\left[\mathcal{T} - \frac{\cos(n\mathcal{T})\sin(n\mathcal{T})}{n}\right]\sin(n\mathcal{T})\varepsilon^3,$$

$$\begin{aligned}
A^e_{31} &= -n\sin(n\mathcal{T}) + \sin(2\theta_0)\sin(n\mathcal{T})\left(n\mathcal{T} + 3\cos(n\mathcal{T})\sin(n\mathcal{T})\right)\varepsilon^3\\
&\quad + 2\Bigg[\sin^2\theta_0\mathcal{T}\left(5 - 8\cos^2(n\mathcal{T})\right)\cos(n\mathcal{T})\\
&\qquad - \frac{\sin(n\mathcal{T})}{n}\left(\cos^2\theta_0\left(8 - 13\cos^2(n\mathcal{T}) + 2\cos^4(n\mathcal{T})\right) + 9\cos^2(n\mathcal{T}) - 6\right)\Bigg]\varepsilon^6
\end{aligned}$$

$$- \frac{2\sin(2\theta_0)}{n}\left[\mathcal{T}\left(1+2\cos^2(n\mathcal{T})\right) - \frac{3\cos(n\mathcal{T})\sin(n\mathcal{T})}{n}\right]\sin^3(n\mathcal{T})\varepsilon^9,$$

$$\begin{aligned} A^e_{32} = &-2\left[n\cos^2\theta_0\mathcal{T} - \left(1+3\sin^2\theta_0\right)\cos(n\mathcal{T})\sin(n\mathcal{T})\right]\sin(n\mathcal{T})\varepsilon^3 \\ &+ \sin(2\theta_0)\left[\mathcal{T}\left(5-8\cos^2(n\mathcal{T})\right) - \frac{8-13\cos^2(n\mathcal{T})+2\cos^4(n\mathcal{T})}{n}\sin(n\mathcal{T})\right]\varepsilon^6 \\ &+ \frac{4\cos^2\theta_0}{n}\left[\mathcal{T}\left(1+2\cos^2(n\mathcal{T})\right) - \frac{3\cos(n\mathcal{T})\sin(n\mathcal{T})}{n}\right]\sin^3(n\mathcal{T})\varepsilon^9, \end{aligned}$$

$$\begin{aligned} A^e_{33} = &\cos(n\mathcal{T}) + \sin(2\theta_0)\left[\mathcal{T}\cos(n\mathcal{T}) + \frac{2-3\cos^2(n\mathcal{T})}{n}\sin(n\mathcal{T})\right]\varepsilon^3 \\ &- \frac{4\cos^2\theta_0}{n}\left[\mathcal{T} - \frac{\cos(n\mathcal{T})\sin(n\mathcal{T})}{n}\right]\sin^3(n\mathcal{T})\varepsilon^6, \end{aligned}$$

$$\begin{aligned} A^e_{34} = &2\left[\sin^2\theta_0\left(\mathcal{T} - \frac{\cos(n\mathcal{T})\sin(n\mathcal{T})}{n}\right)\cos(n\mathcal{T}) + \frac{2\sin^2\theta_0+1}{n}\sin^3(n\mathcal{T})\right]\varepsilon^3 \\ &- \frac{2\sin(2\theta_0)}{n}\left[\mathcal{T} - \frac{\cos(n\mathcal{T})\sin(n\mathcal{T})}{n}\right]\sin^3(n\mathcal{T})\varepsilon^6, \end{aligned}$$

$$\begin{aligned} A^e_{41} = &2\left[n\sin^2\theta_0\mathcal{T} - (1+3\cos^2\theta_0)\cos(n\mathcal{T})\sin(n)\mathcal{T}\right]\sin(n\mathcal{T})\varepsilon^3 \\ &+ \sin(2\theta_0)\left[\mathcal{T}\left(5-8\cos^2(n\mathcal{T})\right) - \frac{8-13\cos^2(n\mathcal{T})+2\cos^4(n\mathcal{T})}{n}\sin(n\mathcal{T})\right]\varepsilon^6 \\ &- \frac{4\sin^2\theta_0}{n}\left[\mathcal{T}\left(1+2\cos^2(n\mathcal{T})\right) - \frac{3\cos(n\mathcal{T})\sin(n\mathcal{T})}{n}\right]\sin^3(n\mathcal{T})\varepsilon^9, \end{aligned}$$

$$\begin{aligned} A^e_{42} = &-n\sin(n\mathcal{T}) - \sin(2\theta_0)\sin(n\mathcal{T})\left(n\mathcal{T}+3\cos(n\mathcal{T})\sin(n\mathcal{T})\right)\varepsilon^3 \\ &+ 2\Bigg[-\cos^2\theta_0\mathcal{T}\left(5-8\cos^2(n\mathcal{T})\right)\cos(n\mathcal{T}) \\ &\quad - \frac{\sin(n\mathcal{T})}{n}\left(\sin^2\theta_0\left(8-13\cos^2(n\mathcal{T})+2\cos^4(n\mathcal{T})\right)+9\cos^2(n\mathcal{T})-6\right)\Bigg]\varepsilon^6 \\ &+ \frac{2\sin(2\theta_0)}{n}\left[\mathcal{T}\left(1+2\cos^2(n\mathcal{T})\right) - \frac{3\cos(n\mathcal{T})\sin(n\mathcal{T})}{n}\right]\sin^3(n\mathcal{T})\varepsilon^9, \end{aligned}$$

$$\begin{aligned} A^e_{43} = &-2\left[\cos^2\theta_0\left(\mathcal{T} - \frac{\cos(n\mathcal{T})\sin(n\mathcal{T})}{n}\right)\cos(n\mathcal{T}) + \frac{2\cos^2\theta_0+1}{n}\sin^3(n\mathcal{T})\right]\varepsilon^3 \\ &- \frac{2\sin(2\theta_0)}{n}\left[\mathcal{T} - \frac{\cos(n\mathcal{T})\sin(n\mathcal{T})}{n}\right]\sin^3(n\mathcal{T})\varepsilon^6, \end{aligned}$$

$$\begin{aligned} A^e_{44} = &\cos(n\mathcal{T}) - \sin(2\theta_0)\left[\mathcal{T}\cos(n\mathcal{T}) + \frac{2-3\cos^2(n\mathcal{T})}{n}\sin(n\mathcal{T})\right]\varepsilon^3 \\ &- \frac{4\sin^2\theta_0}{n}\left[\mathcal{T} - \frac{\cos(n\mathcal{T})\sin(n\mathcal{T})}{n}\right]\sin^3(n\mathcal{T})\varepsilon^6. \end{aligned}$$

References

[1] J. Zakrzewki, D. Delande, J.C. Gay, Ionization of highly excited hydrogen atoms by a circularly polarized microwave field, Phys. Rev. A 47 (1993) 2468–2471, http://dx.doi.org/10.1103/PhysRevA.47.R2468.

[2] A. Buchleitner, D. Delande, J.C. Gay, Microwave ionization of three-dimensional hydrogen atoms in a realistic numerical experiment, J. Opt. Soc. Amer. B 4 (1995) 505–519, http://dx.doi.org/10.1364/JOSAB.12.000505.

[3] A.F. Brunello, T. Uzer, D. Farrelly, Hydrogen atom in circularly polarized microwaves: Chaotic ionization via core scattering, Phys. Rev. A 55/5 (1997) 3730–3745, http://dx.doi.org/10.1103/PhysRevA.55.3730.

[4] Charles Jaffé, D. Farrelly, T. Uzer, Transition state theory without time-reversal symmetry: Chaotic ionization of the hydrogen atom, Phys. Rev. Lett. 84 (2000) 610–613, http://dx.doi.org/10.1103/PhysRevLett.84.610.

[5] E. Barrabés, M. Ollé, F. Borondo, D. Farrelly, Mondelo J.M., Phase space structure of the hydrogen atom in a circularly polarized microwave field, Physica D 241/4 (2012) 333–349, http://dx.doi.org/10.1016/j.physd.2011.10.016.

[6] R. McGehee, Triple collision in the collinear three-body problem, Invent. Math. 27 (1974) 191–227, http://dx.doi.org/10.1007/BF01390175.

[7] R. McGehee, Singularities in classical celestial mechanics, in: Proceedings of the International Congress of Mathematicians Helsinki, 1978, pp. 827–834.

[8] M. Ollé, To and fro motion for the hydrogen atom in a circularly polarized microwave field, Commun. Nonlinear Sci. Numer. Simul. 54 (2018) 286–301, http://dx.doi.org/10.1016/j.cnsns.2017.05.026.

[9] M. Alvarez-Ramírez, C. Vidal, Behavior of the binary collision in a planar restricted (n+1)-body problem, Physica D 254 (2013) 1–11, http://dx.doi.org/10.1016/j.physd.2013.02.012.

[10] A. Chenciner, J. Llibre, A note on the existence of invariant punctured tori in the planar circular restricted three-body problem, Ergodic Theory Dynam. Systems 8 (1988) 63–72, http://dx.doi.org/10.1017/s0143385700009330.
[11] J. Delgado Fernández, Transversal ejection-collision orbits in Hill's problem for C>>1, Celestial Mech. Dynam. Astronom. 44 (1988) 299–307, http://dx.doi.org/10.1007/bf01235542.
[12] E.A. Lacomba, J. Llibre, Transversal ejection-collision orbits for the restricted problem and the Hill's problem with applications, J. Differential Equations 74 (1988) 69–85, http://dx.doi.org/10.1016/0022-0396(88)90019-8.
[13] J. Llibre, J. Martínez Alfaro, Ejection and collision orbits of the spatial restricted three-body problem, Celestial Mech. Dynam. Astronom. 35 (1985) 113–128, http://dx.doi.org/10.1007/bf01227665.
[14] D.L. Maranhão, J. Llibre, Ejection–collision orbits and invariant punctured tori in a restricted four-body problem, Celestial Mech. Dynam. Astronom. 71 (1998) 1–14, http://dx.doi.org/10.1023/a:1008389427687.
[15] C. Piñol, Ejection-collision orbits with the more massive primary in the planar elliptic restricted three body problem, Celestial Mech. Dynam. Astronom. 61 (1995) 315–331, http://dx.doi.org/10.1007/bf00049513.
[16] M. Ollé, O. Rodríguez, J. Soler, Analytical and numerical results on families of n-ejection-collision orbits in the RTBP, Commun. Nonlinear Sci. Numer. Simul. 90 (2020) http://dx.doi.org/10.1016/j.cnsns.2020.105294.
[17] M. Ollé, O. Rodríguez, J. Soler, Transit regions and ejection/collision orbits in the RTBP, Commun. Nonlinear Sci. Numer. Simul. 94 (2021) http://dx.doi.org/10.1016/j.cnsns.2020.105550.
[18] M. Ollé, Ó. Rodríguez, J. Soler, Study of the ejection/collision orbits in the spatial RTBP using the McGehee regularization, Commun. Nonlinear Sci. Numer. Simul. 111 (2022) http://dx.doi.org/10.1016/j.cnsns.2022.106410.
[19] T. Martínez-Seara, M. Ollé, Ó. Rodríguez, J. Soler, Generalized analytical results on n-ejection–collision orbits in the RTBP. Analysis of bifurcations, J. Nonlinear Sci. 33 (1) (2023) http://dx.doi.org/10.1007/s00332-022-09873-y.
[20] M.J. Capinski, S. Kepley, J.D. Mireles James, Computer assisted proofs for transverse collision and near collision orbits in the restricted three body problem, 2022, http://dx.doi.org/10.48550/arXiv.2205.03922, Preprint.
[21] A. Boscaggin, R. Ortega, L. Zhao, Periodic solutions and regularization of a Kepler problem with time-dependent perturbation, Trans. Amer. Math. Soc. 372 (2019) 677–703, http://dx.doi.org/10.1090/tran/7589.
[22] R. Ortega, L. Zhao, Generalized periodic orbits in some restricted three-body problems, Z. Angew. Math. Phys. 72 (2021) http://dx.doi.org/10.1007/s00033-021-01470-5.
[23] E. Fehlberg, Classical fifth, sixth, seventh and eighth order Runge–Kutta formulas with stepsize control, Tech. rep., NASA, R-287, 1968.
[24] J.H. Verner, Explicit Runge–Kutta methods with estimates of the local truncation error, SIAM J. Numer. Anal. 15 (1978) 772–790, http://dx.doi.org/10.1137/0715051.
[25] J.R. Dormand, J.P. Prince, A family of embedded Runge–Kutta formulae, J. Comput. Appl. Math. 6 (1) (1980) 19–26, http://dx.doi.org/10.1016/0771-050X(80)90013-3.
[26] A. Jorba, Zou. M., A software package for the numerical integration of ODE's by means of high-order taylor methods, Experiment. Math. 14 (1982) 99–117, http://dx.doi.org/10.1103/PhysRevLett.84.610.
[27] K.R. Meyer, G.R. Hall, Introduction To Hamiltonian Dynamical Systems and the N-Body Problem, in: Applied Mathematical Sciences (Switzerland) 90, Springer New York, 1992.
[28] M. Ollé, J.R. Pacha, Hopf bifurcation for the hydrogen atom in a circularly polarized microwave field, Commun. Nonlinear Sci. Numer. Simul. 62 (2018) 27–60, http://dx.doi.org/10.1016/j.cnsns.2018.02.005.
[29] Ó. Rodríguez, Ejection-Collision Orbits in the Restricted Three-Body Problem, UPC, 2021.
[30] Donald G. Saari, Collisions, Rings, and Other Newtonian N-Body Problems, vol. 104, Published for the Conference Board of the Mathematical Sciences, Washington, DC; by the American Mathematical Society, Providence, RI, 2005, p. x+235.